

**UNIVERSITÀ DEGLI STUDI DI NAPOLI “FEDERICO II”**



**SCUOLA POLITECNICA E DELLE SCIENZE DI BASE**

**DIPARTIMENTO DI INGEGNERIA INDUSTRIALE**

**TESI DI LAUREA IN INGEGNERIA AEROSPAZIALE**

**ESTIMATION OF INCREASE IN LIFT AND DRAG COEFFICIENTS RELATIVE TO USAGE  
OF HIGH LIFT DEVICES AT TAKE-OFF AND LANDING**

**RELATORE**

**FABRIZIO NICOLosi**

**CANDIDATI**

**CIRO BAIA**

**DARIO DE ROSA**

**ANNO ACCADEMICO 2014/2015**

# Table of contents

<b>1 The influence of high-lift systems on the stall.....</b>	<b>3</b>
1.1 Take-off Requirements.....	4
1.2 Landing Requirements.....	5
<b>2 High-Lift systems: flaps and slats.....</b>	<b>7</b>
2.1 Trailing edge devices.....	9
2.1.1 Split flap.....	9
2.1.2 Single slotted flap.....	10
2.1.3 Double slotted flap.....	10
2.1.4 Triple slotted flap.....	12
2.1.5 Single slotted Fowler flap.....	12
2.1.6 Plain flap.....	13
2.2 Leading edge devices.....	13
2.2.1 Slat.....	13
2.2.2 Krueger flap.....	14
2.2.3 Plain leading edge flap.....	14
<b>3 Variation of lift coefficient .....</b>	<b>15</b>
3.1 Variation of lift coefficient at zero angle of attack.....	16
3.1.1 Determination of $\Delta C_{l,0}$ for the airfoil due to flap extension.....	16
3.1.2 Determination of $\Delta C_{L,0}$ for the wing due to flap extension.....	18
3.2 Variation of maximum lift coefficient.....	19
3.2.1 Determination of $\Delta C_{l,max}$ for the airfoil due to T. E. devices.....	19
3.2.2 Determination of $\Delta C_{l,max}$ for the airfoil due to L. E. devices.....	20
3.2.3 Determination of $\Delta C_{L,max}$ for the wing due to T. E. devices.....	23
3.2.4 Determination of $\Delta C_{L,max}$ for the wing due to L. E. devices.....	23
3.3 Variation of lift gradient due to flap deflection.....	24
3.4 Variation of drag coefficient due to high lift devices.....	24
<b>4 Application on general-aviation aircrafts.....</b>	<b>25</b>
4.1 Boeing 737.....	26
4.1.1 Graphical and numerical results for take-off computations.....	28
4.1.2 Graphical and numerical results for landing computations.....	29
4.2 ATR 42.....	30
4.2.1 Graphical and numerical results for take-off computations.....	32
4.2.2 Graphical and numerical results for landing computations.....	33
<b>Appendix A .....</b>	<b>34</b>
<b>Appendix B .....</b>	<b>40</b>

# 1 The influence of high-lift systems on the stall

In fluid dynamics, a stall is a reduction of the lift coefficient due to an increase of the angle of attack or due to a decrease of speed incident on a wing profile.

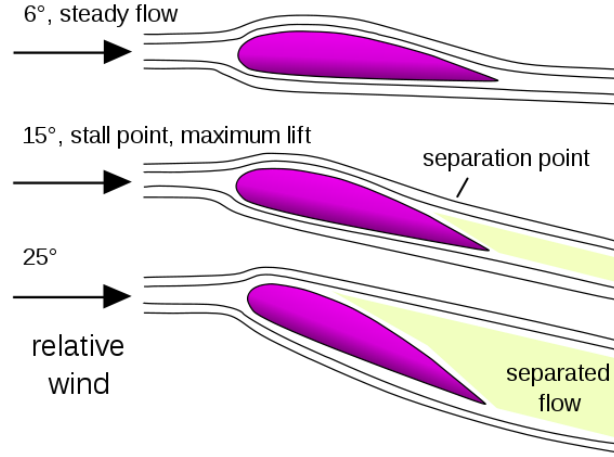


Figure 1: boundary layer separation at the stall

The stall happens when the point of flow separation on the upper wing is so advanced to cause flow separation over most of the upper wing. The flow separates due to the adverse pressure gradients, for this reason to improve performances of an airfoil about the stall is necessary to delay the progress of the separation point. To solve the stall inconvenience, all aircraft are equipped of high-lift systems, used during take-off and landing.

A parameter that describes the stall is the stalling speed, expressed by the following equation:

$$V_{stall} = \sqrt{\frac{2 W}{\rho S C_{L_{max}}}} \quad (1)$$

- $W$  is the weight of the aircraft
- $S$  is the wing surface
- $\rho$  is the air density
- $C_{L_{max}}$  is the aircraft maximum lift coefficient

The altitude ( $\rho$ ) and the wing-load ( $\frac{W}{S}$ ) are given parameters, so the only way to vary stalling speed is altering  $C_{L_{max}}$ .

Stalling speed is the minimum speed at which an aircraft can fly without losing altitude, for this reason the only way to decrease stalling speed is increasing  $C_{L_{max}}$ .

## 1.1 Take-off Requirements

Take-off is the expression used to refer to a series of phases:

- **Taxiing phase:** the aircraft accelerates from zero speed to the *rotation speed*
- **Rotation phase:** the pilot acts on elevator to increase angle of attack, so lift exceeds weight and generates a vertical acceleration
- **Climb phase before passing the obstacle:** the aircraft reaches a safe altitude, about 1500 ft, to which succeeds the phase of climb to cruising altitude

Length of take-off is the length of the projection of the trajectory on the runway that the aircraft performs from stationary conditions to the overcoming of the imaginary obstacle, situated at 35 ft for civil aircraft, established by the norm JAR/FAR 25 (Joint/Federal Aviation Requirements).

During take-off the aircraft must have a  $V_{LO}$ , that is the speed at which the aircraft leaves the ground, equal to  $1.2 V_{S-TO}$  (JAR/FAR 25.107)

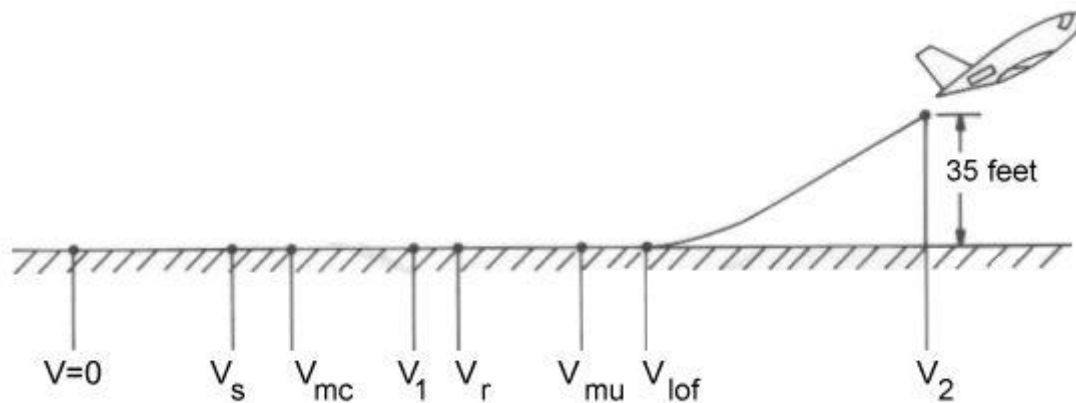


Figure 2: take-off speeds

Speed	Description	FAR 25 Requirement
$V_{S-TO}$	Stall speed in take-off configuration	-
$V_{mc}$	Minimum control speed with one engine inoperative (OEI)	-
$V_1$	OEI decision speed	$= \text{ or } > V_{mc}$
$V_r$	Rotation speed	$5\% > V_{mc}$
$V_{mu}$	Minimum unstick speed for safe flight	$= \text{ or } > V_s$
$V_{LO}$	Lift-off speed	$10\% > V_{mu}$ $5\% > V_{mu} \text{ (OEI)}$
$V_2$	Take-off climb speed at 35 ft	$20\% > V_s$ $10\% > V_{mc}$

The expression of the ground roll distance  $S_G$  shows the relationship between the runway length and the aircraft high-lift characteristics:

$$S_G = \int_0^{V_{LO}} dS = \int_0^{V_{LO}} \frac{V}{a} dV = \frac{1}{2} \int_0^{V_{LO}} \frac{1}{a} d(V^2)$$

The final expression, obtained by simplifications is:

$$S_G = \frac{W}{2g} K^2 \frac{W}{S} \frac{2}{\rho} \frac{1}{[T - D - \mu(W - L)]} \frac{1}{0,7V_{LO} C_{L_{max-T0}}} \quad (2)$$

Where:

$$a = \frac{g}{W} [T - D - \mu(W - L)]$$

$$V_{LO} = KV_S \quad \text{with } K=1.2$$

## 1.2 Landing Requirements

Landing is a group of phases through which the aircraft passes from the air to the ground with zero speed.

According to JAR 23 and JAR 25, the landing starts when the aircraft is located at a conventional altitude of 50 ft, and length of landing is the horizontal length covered to stop, starting from the conventional obstacle.

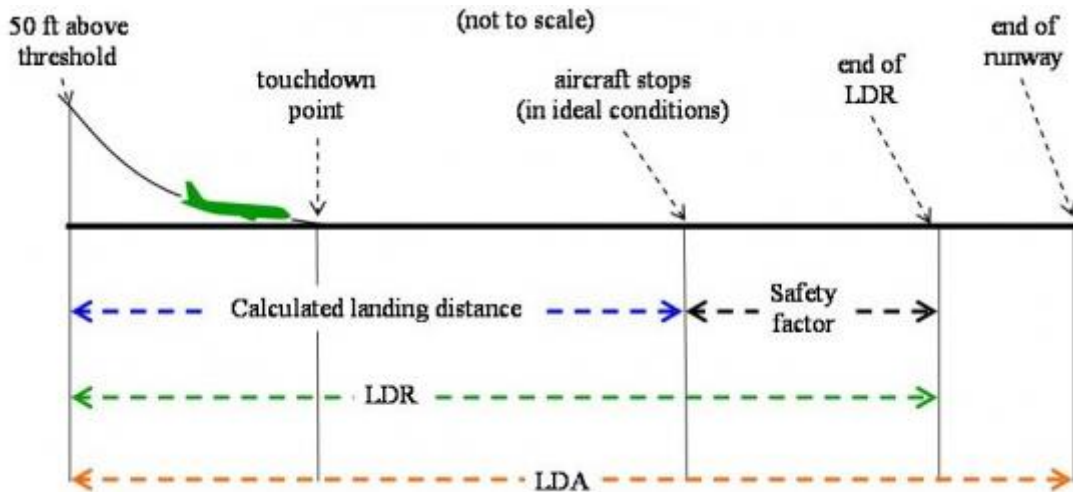


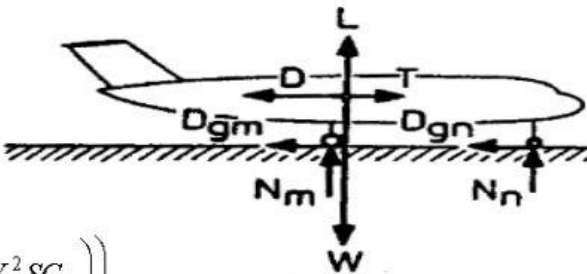
Figure 3: landing phases

**LDA** Landing Distance Available

**LDR** Landing Distance Required

- The speed must be between  $V_{L1}$  and  $V_{L2}$  when touching the ground in landing (JAR/FAR 25.479) where  $V_{L1}$  and  $V_{L2}$  are obtained substituting the weight of the aircraft in landing conditions and the **ISA** “sea level standard” and **ISA** “hot day” respectively in the stalling speed equation
- When approaching the runway before the reference obstacle, the speed must be higher than  $1.3V_S$  (JAR 25.119)

The expression of the ground roll distance  $S_G$  shows the relationship between the runway length and the aircraft high-lift characteristics:



$$W = L + N_m + N_n = L + N$$

$$m \frac{dV}{dt} = T - D - D_{gm} - D_{gn} = T - D - D_g$$

$$\frac{dV}{dt} = a = \frac{1}{m} \left( T - \frac{1}{2} \rho V^2 S C_D - \mu \left( W - \frac{1}{2} \rho V^2 S C_L \right) \right)$$

$$dS_G = V dt = \frac{V}{a} dV = \frac{mV dV}{\left( T - \frac{1}{2} \rho V^2 S C_D - \mu \left( W - \frac{1}{2} \rho V^2 S C_L \right) \right)}$$

$$S_G = \int_0^{S_G} ds = \int_{V_r}^0 \frac{V}{a} dV = \int_{V_r}^0 \frac{mV}{\left( T - \mu W - \frac{1}{2} \rho V^2 S (C_D - \mu C_L) \right)} dV$$

The final expression, obtained by simplifications is:

$$S_G = \frac{W}{2g} K_L^2 \frac{W}{S} \frac{2}{\rho} \frac{1}{[T - D - \mu(W - L)]} \frac{1}{0,7V_{TD} C_{L_{max-L}}} \quad (3)$$

Where:

$$a = \frac{g}{W} [T - D - \mu(W - L)] \quad V_{TD} = K_L V_{S-L} \quad \text{with } K_L = 1.1$$

$V_{TD}$  is the speed at touch-down and  $C_{L_{max-L}}$  is the maximum lift coefficient in landing, which is higher than the one in take-off because of the consequent increment in  $C_D$ .

## 2 High-Lift systems: flaps and slats

The need to limit the runway length to have a safer take-off and landing has as consequence the aim of designing aircrafts with a low speed on the ground.

This decrease in speed influences lift, so aircraft loses its capability to sustain itself through the air, and increasing angle of attack, it would accentuate the stall.

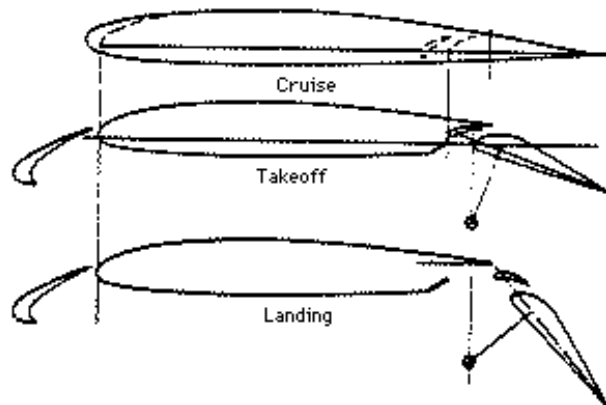


Figure 4: High Lift devices deflections at cruise, take-off and landing

To assure high lift in take-off and landing without varying weight and wing surface, we work on airfoil shape, for this reasons high-lift systems are used. High-lift systems are commonly defined as the devices that allow to increase the maximum lift coefficient ( $C_{L_{max}}$ ) of the aircraft and consequently to decrease the stalling speeds ( $V_{S-TO}$ ,  $V_{S-L}$ ). A great part of High-lift systems works modifying wing shape extracting moving surfaces, but some of them act directly on the flow trying to control it, just like as *Blown Flaps* or *Jet Flaps*. A typical division can be made between *Leading-Edge Devices* that are located in the forward part of the wing (leading edge of the airfoil), and *Trailing-Edge Devices* that are located in the rear side of the wing. These kind of High-Lift systems have different effects on the aerodynamic characteristics due to their position relative to the airfoil main element, their shape and geometry.

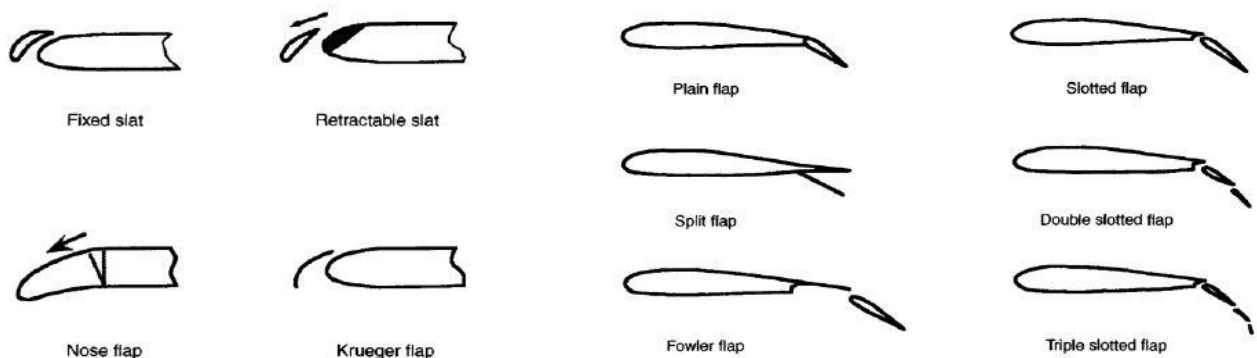
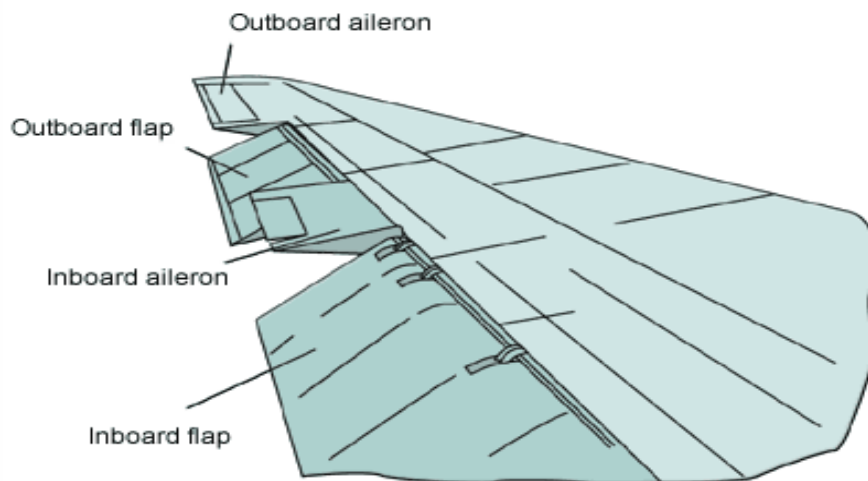


Figure 5: different kind of High Lift devices

- **Trailing edge devices (flaps):** these devices produce an increase of airfoil curvature. In standard condition they are the airfoil trailing edge, however when speed decreases, they rotate downwards. A particular kind of flap is the slotted one, this device has almost two other important effects: the first is to generate an airfoil extension, and the second is delaying stall through some slots between upper and lower wing; flux flows through these slots energizing the area affected by the separation of the boundary layer.



*Figure 6: trailing edge devices*

- **Leading edge devices (slats or flaps):** these devices allow the access of the flow to the upper wing to reduce the expansion of pressure in order to delay separation of boundary layer. Modern airliners generally are equipped with slats since they are relatively simple and provide lift augmentation with little drag penalty. The feature differentiating leading edge flaps from slats is that the former have their trailing portions coincident with the airfoil surface so that there is no slot formed as there is in a leading edge slat system.

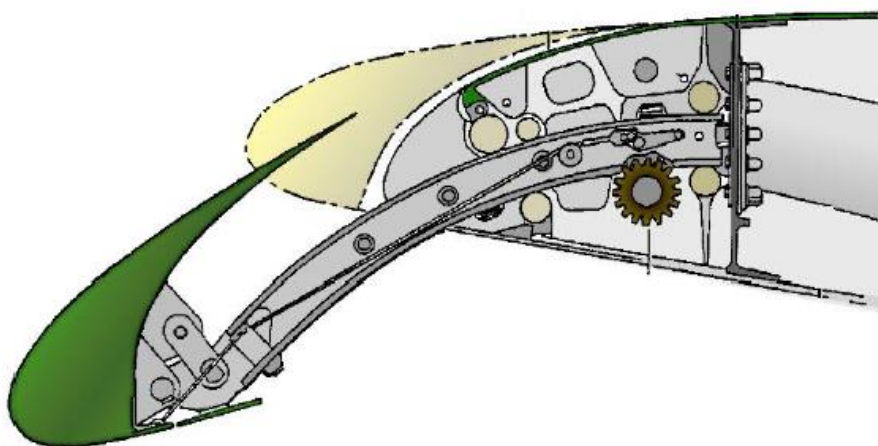


*Figure 7: leading edge device*



- **Slot and slat effect on lift:** these systems influence boundary layer control, in fact they introduce a *blowing* that energizes the boundary layer delaying separation, so an increase in lift is generated.

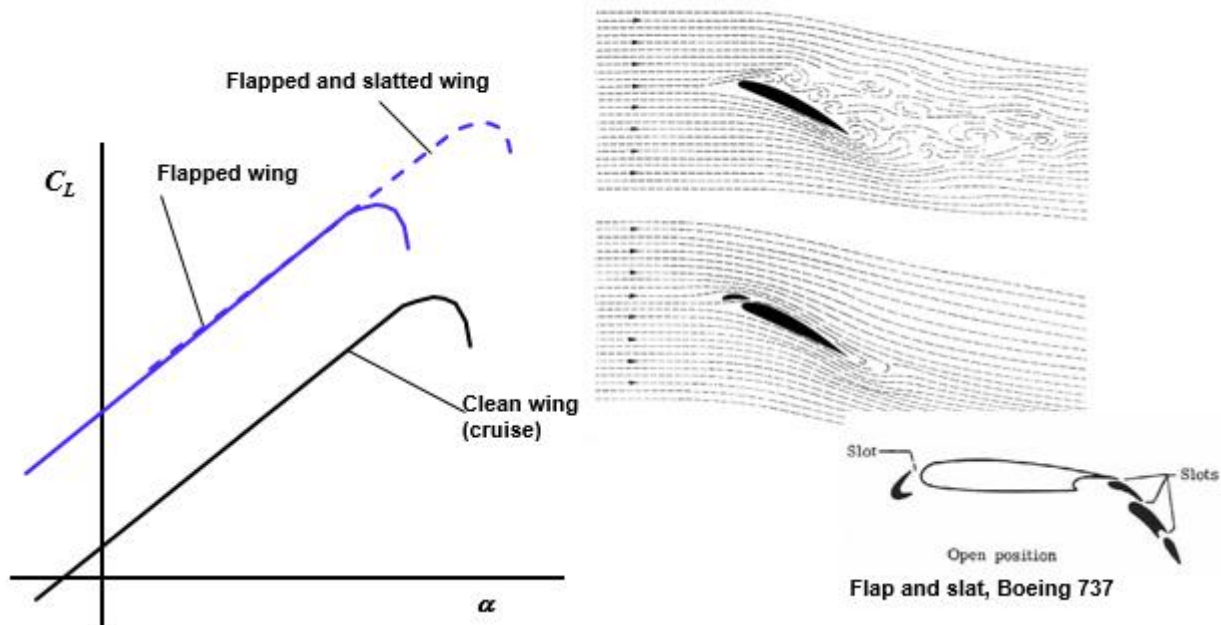


Figure 8: slot and slat effect on lift

## 2.1 Trailing edge devices

Among *trailing edge devices*, we list the noteworthy ones:

**2.1.1 Split flap:** it consists of a stiffened plate on the lower surface, hinged just aft of the rear spar, by means of a piano hinge. The drag due to flap deflection is large, particularly in the case of small deflections, thus making the split flap less suitable for take-off. Although its structural simplicity and low weight are attractive, this type of flap must now be considered as obsolete.

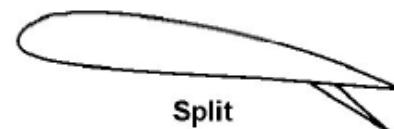
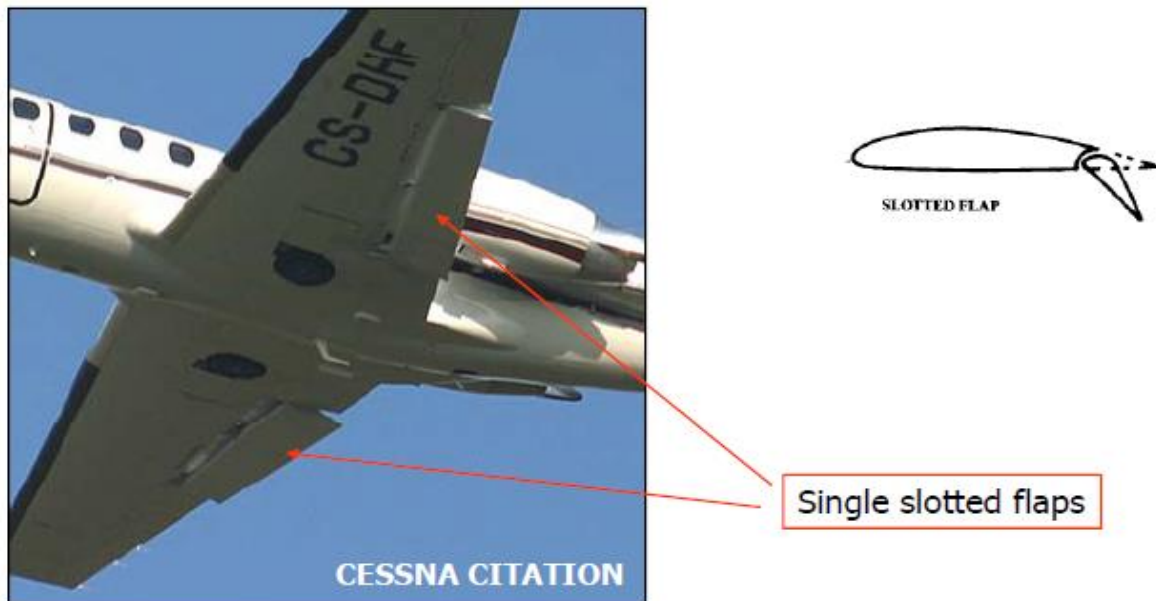


Figure 9: split flap

**2.1.2 Single slotted flap:** it can be seen as a plain flap with a gap between the two elements composing the airfoil. The single slotted flap has very little flap overlap with the fixed trailing edge and hence develops only little Fowler motion, that is the aft travel of the flap that increases the section chord.

The effects of a single slotted flap show an increment in all the aerodynamic coefficients ( $C_L$ ,  $C_D$ ,  $C_m$ ), but it must be said that the increment in drag is lower than that for plain or split flaps. The slotted flap chord usually ranges from the 25% up to the 30% of the section chord.



*Figure 10: single slotted flap*

**2.1.3 Double slotted flap:** this device is superior to the previous type at large deflections, because separation of the flow over the flap is postponed by the more favourable pressure distribution.

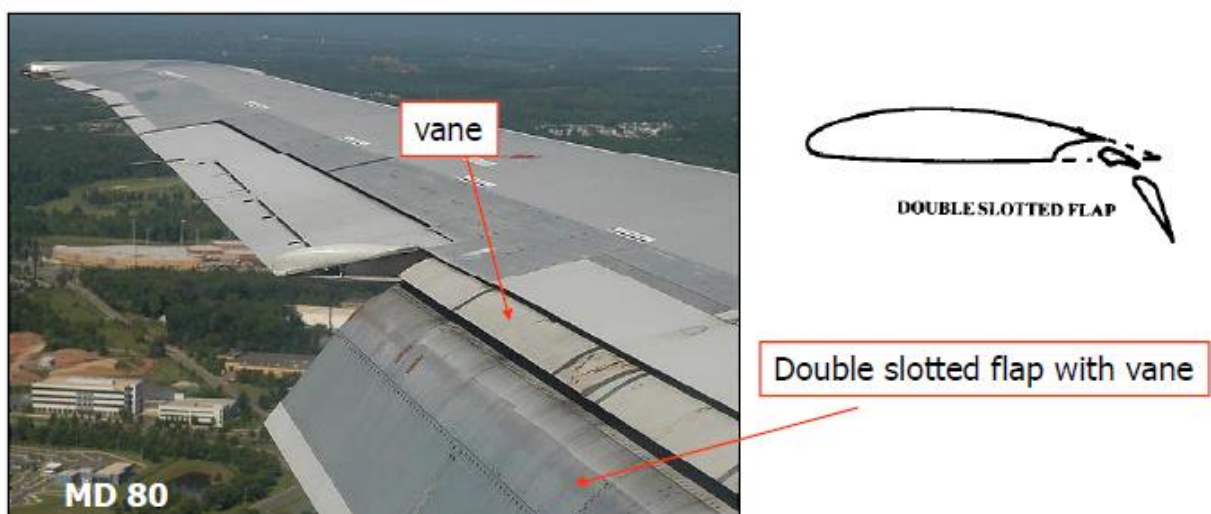


*Figure 11: double slotted flap*

Various degrees of mechanical sophistication are possible:

1. Flaps with a fixed hinge and a fixed vane of relatively small dimensions are structurally simple but may have high profile drag during take-off.

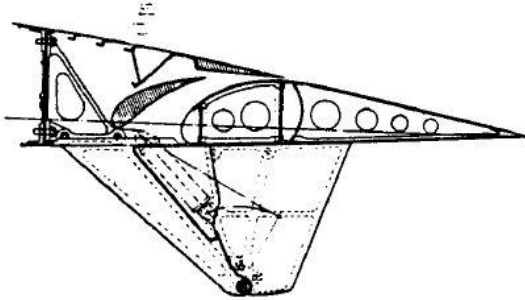


*Figure 11.1*

2. Double slotted flaps may be supported on a four-bar mechanism. During extension the slot shape closely approximates to the aerodynamic optimum, but the flap supports cause a disturbance in the flow through the slot.

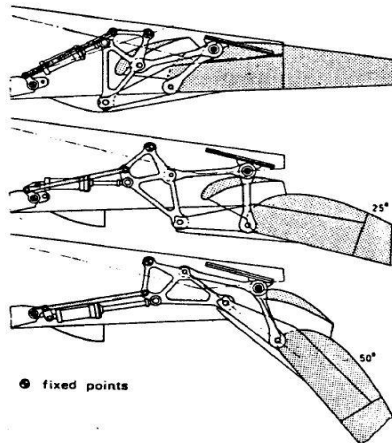


*Figure 11.2*

3. If the two flap elements are independently adjustable, the maximum deflection may be increased up to 70 degrees.

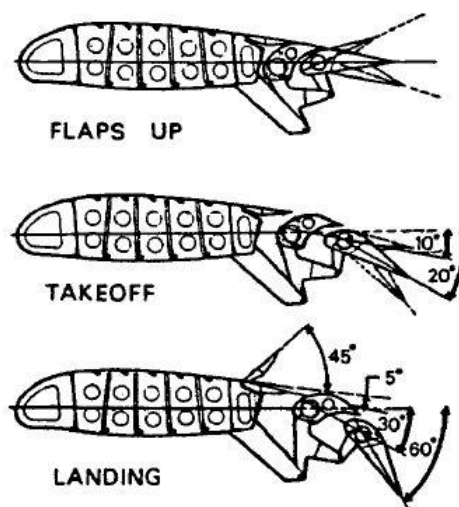


*Figure 11.3*

**2.1.4 Triple slotted flap:** this device is used on several transport aircraft with very high wing loadings. In combination with leading edge devices, this system represents almost the ultimate achievement in passive high-lift technology, but its shape shows that complicated flap supports and controls are required.



*Figure 12: triple slotted flap*

**2.1.5 Single slotted fowler flap:** it is theoretically a single slotted flap that adds to the downward deflection also a backward motion that allows the increment of the effective chord and camber.

Due to the necessity of keeping the rear part of the wing section extended out the main element its implementation system is usually more complicated than the single slotted flaps but its weight and costs are largely justified by its high lift effectiveness.

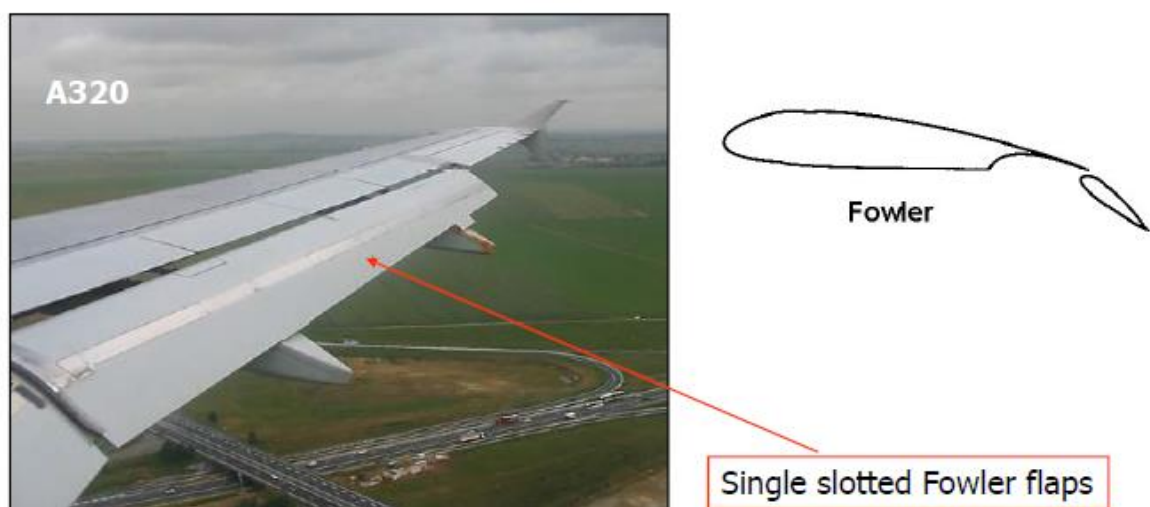


*Figure 13: single slotted fowler flap*



**2.1.6 Plain flap:** this device is most used on small aircraft or ones equipped of a thin wing because it doesn't support a complex mechanism of retraction. Typical deflections are about  $20^\circ$  for take-off and  $60^\circ$  for landing.



Figure 14: plain flap

## 2.2 Leading edge devices

Among *leading edge devices*, we list the noteworthy ones:

**2.2.1 Slat:** is small, highly cambered airfoil foreword of the wing leading edge, which experiences large suction forces per unit of area and reduces the suction forces on the basic airfoil. In its intermediate take-off position, the slat is at a low angle, with his trailing edge sealed against the upper surface of the fixed leading edge for the best L/D performance.

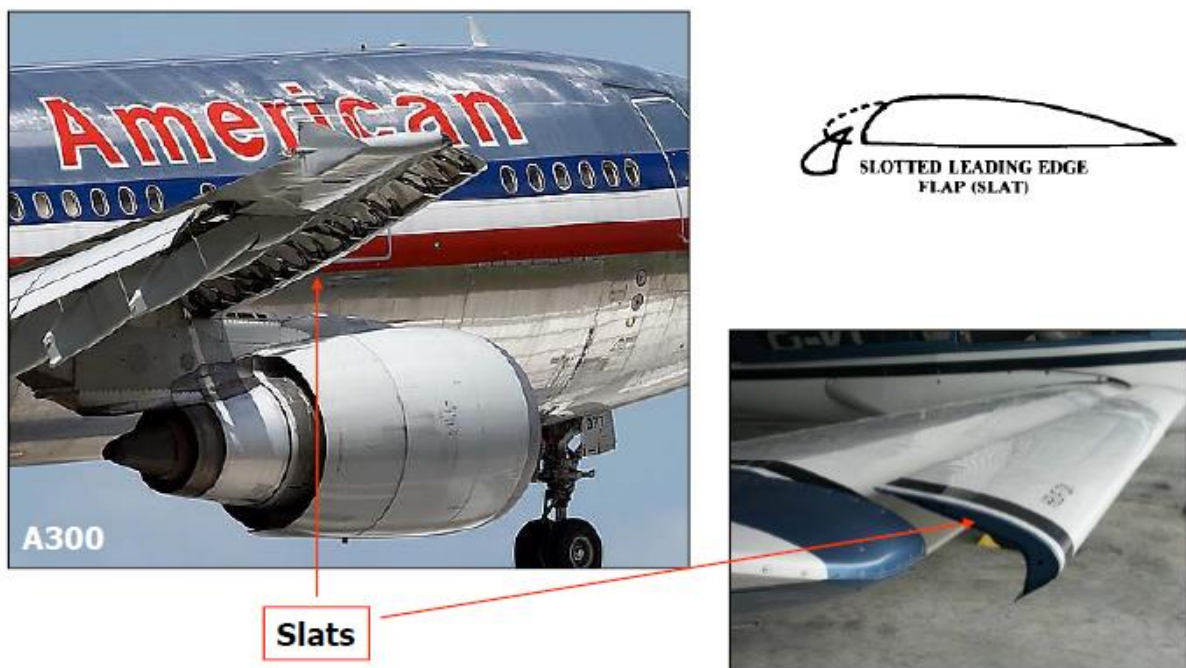
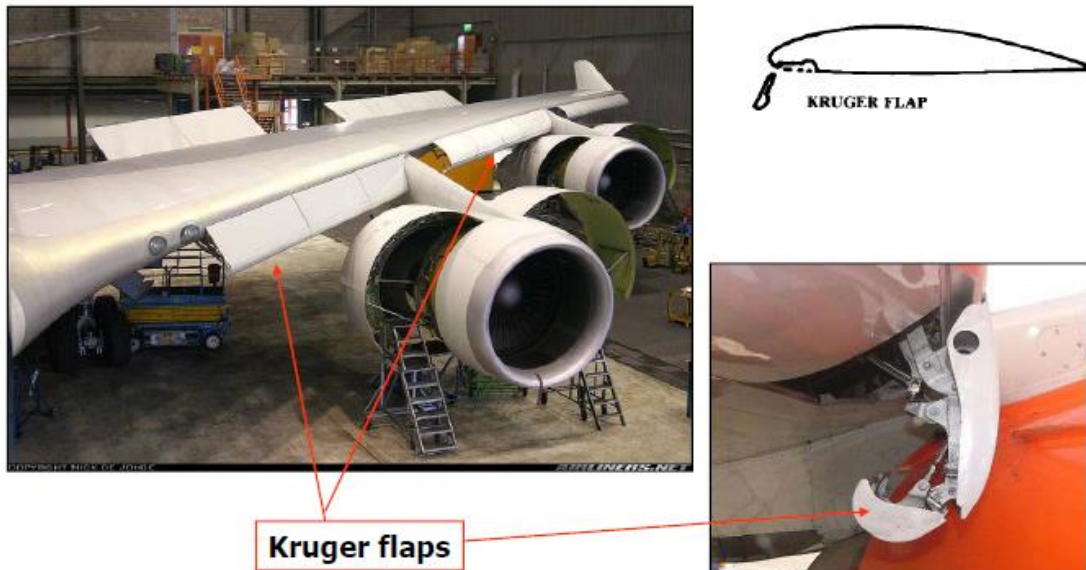


Figure 15: slat

**2.2.2 Krueger flap:** it performs in the same way as slat, but it is thinner and more suitable for installation on thin wings. Krueger flaps are used on the inboard part of wings, in combination with outboard slats, to obtain positive longitudinal in the stall.



*Figure 16: Krueger flaps*

**2.2.3 Plain leading edge flap:** is less effective than slat, it is mechanically simple and rigid and particularly suitable for thin airfoil sections. The leading edge can be hinged in order to move it backward (droop nose) or it has a mechanism inside that changes the curvature of the nose (variable camber flap).

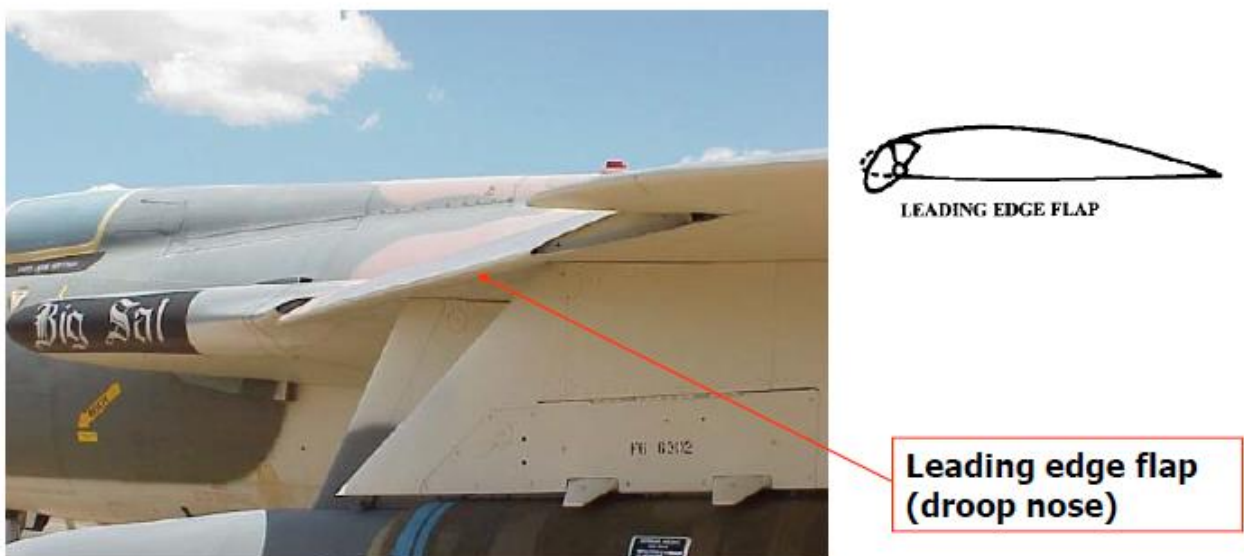


*Figure 17: droop nose*

### 3 Variation of lift coefficient

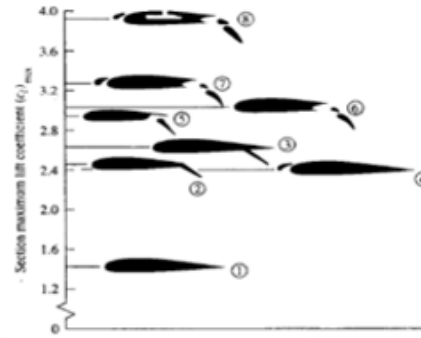
The deployment of a trailing edge flap changes the camber of the airfoil, it increases the maximum lift coefficient and decreases the zero-lift angle of attack.

The lift-angle of attack curve with flaps deflected can be drawn from the curve with flap retracted after the computation of three terms:

$\Delta C_{l,0}$ : The variation of  $C_l$  when the airfoil is at zero angle of attack.

$\Delta C_{l,max}$ : The variation of  $C_l$  when the airfoil is at the angle of attack of stall.

Table below contains typical values of  $C_{l,max}$  for an airfoil at standard angle of attack during take-off and landing

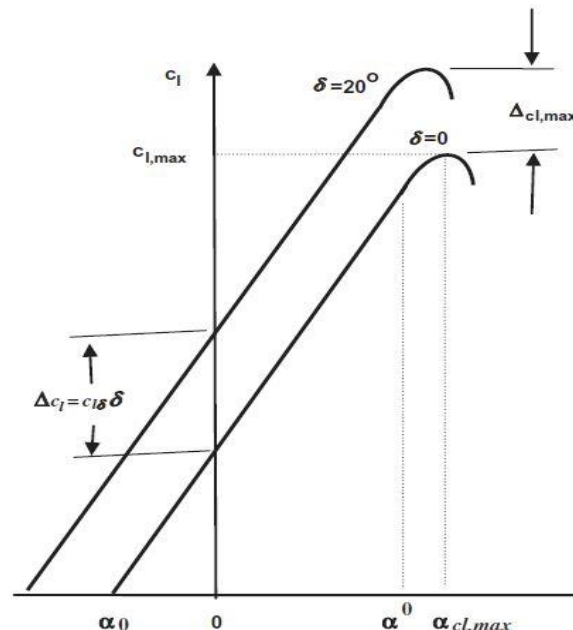


High-Lift Device		Typical Flap Angle		$(C_{l,max})_{\cos \Lambda}$	
Trailing Edge	Leading Edge	Takeoff	Landing	Takeoff	Landing
Plain flap		20°	60°	1.4-1.6	1.7-2.0
Single-slotted flap		20°	40°	1.5-1.7	1.8-2.2
Fowler flap					
single-slotted		15°	40°	2.0-2.2	2.5-2.9
double-slotted		20°	50°	1.7-1.95	2.3-2.7
double-slotted	slat	20°	50°	2.3-2.6	2.8-3.2
triple-slotted	slat	20°	40°	2.4-2.7	3.2-3.5

Figure 18: typical values of  $C_{l,max}$  for an airfoil

$C_{l,\alpha,f}$ : The lift gradient when flap is deflected.

These terms are very sensitive to the type of flap used in the configuration chosen.

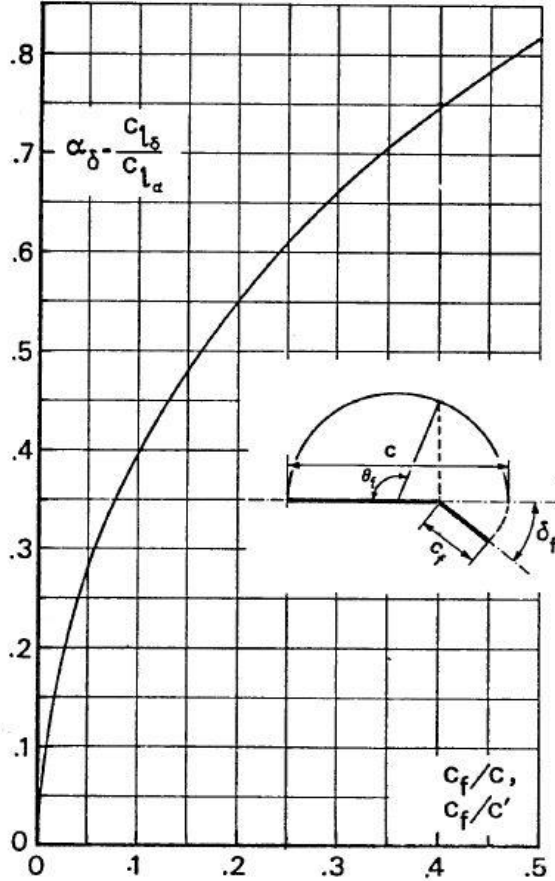


The generic change in the lift curve of an airfoil when a trailing edge flap is deflected

### 3.1 Variation of lift coefficient at zero angle of attack

#### 3.1.1 Determination of $\Delta C_{l,0}$ for the airfoil due to flap extension

An empirical method for predicting airfoil lift increments at zero angle of attack for high-lift systems comes from the Glauert's linearized theory for thin airfoils with flaps. A result obtained from this theory for the lift due to flap deflection is:



$$\alpha_\delta = \frac{\partial \alpha}{\partial \delta_f} = 1 - \frac{\theta_f - \sin \theta_f}{\pi}$$

rate of change of zero lift angle of attack due to flap deflection.

Where:

$$\theta_f = \cos^{-1} \left( 2 \frac{c_f}{c} - 1 \right)$$

Figure 19: Flap lift factor-flapped chord relation

When flaps are deflected, there is an increment of lift valued by the equation:

$$\Delta C_{l,0} = \alpha_\delta C_{l\alpha} \delta_f \quad \begin{array}{l} C_{l\alpha} \text{ is the variation of } C_l \text{ in the clean configuration compared to angle of attack;} \\ \delta_f \text{ is the flap angular deflection.} \end{array}$$

For large flap deflections and for the separation at large flap angles due to viscosity, linear theory is in error when compared with exact one, for this reason we assume the effectiveness factor  $\eta_\delta$ , so the formulation becomes:

$$\Delta C_{l,0} = \alpha_\delta C_{l\alpha} \delta_f \eta_\delta \quad (4)$$



The lift effectiveness factor  $\eta_\delta$  depends on flap type as shown below

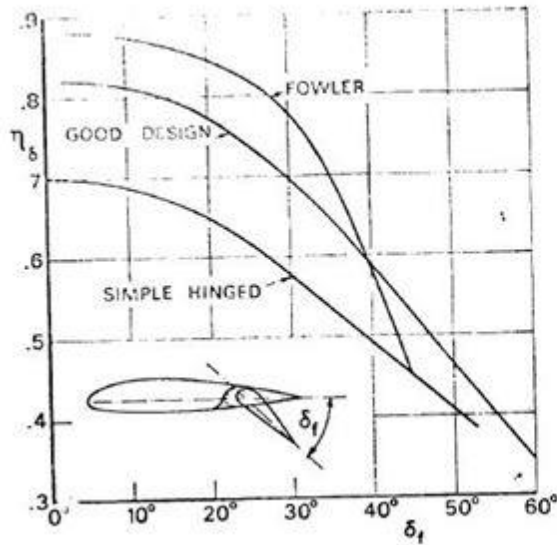


Figure 20:

$\eta_\delta$  for Single Slotted Fowler, Single Slotted Simple Hinged Flaps

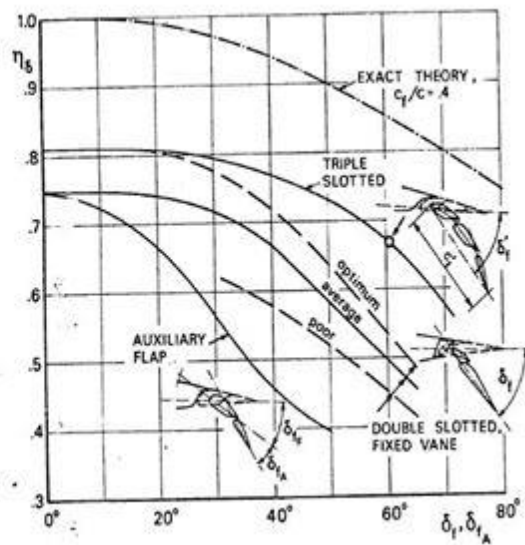
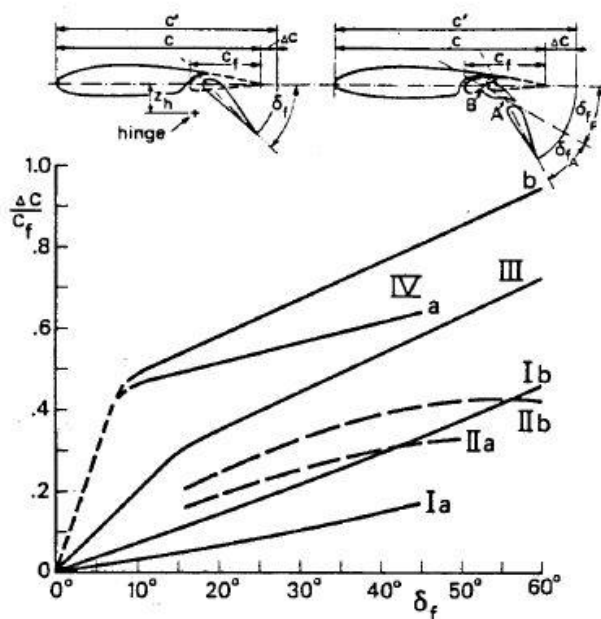


Figure 21:

$\eta_\delta$  for Multi-Elements flaps

For a given flap geometry and type of support, the amount of chord extension can be calculated from the graph below, in absence of other informations:



- I: Fixed hinge - a:  $z_h/c_f = .2$   
b:  $z_h/c_f = .4$
- II: Typical optimum flap position  
a: single slotted  
b: double slotted, fixed vane
- III: Double slotted, variable geometry, with flap extension
- IV: Fowler - a: single slotted, double slotted with fixed vane  
b: double and triple slotted, with flap extension

Figure 22: Extension of the chord depending on flap type

The extended chord is valued as follows:  $\frac{c'}{c} = 1 + \frac{\Delta c}{c_f} \frac{c_f}{c}$

Thus, the equation of  $\Delta C_{l,0}$ , influenced by chord extension is:  $\Delta C'_{l,0} = \alpha'_{\delta} C_{l\alpha} \delta_f \eta_{\delta}$

The result is converted to the initial chord by the following equation:

$$\Delta C_{l,0} = \Delta C'_{l,0} \frac{c'}{c} + C_{l,0} \left( \frac{c'}{c} - 1 \right) \quad (5)$$

### 3.1.2 Determination of $\Delta C_{L,0}$ for the wing due to flap extension

The equation that allow to flit from 2D formulation to 3D one, is:

$$\Delta C_{L,0} = \Delta C_{l,0} \left( \frac{C_{L\alpha}}{C_{l\alpha}} \right) \left[ \frac{(\alpha_{\delta})_{C_L}}{(\alpha_{\delta})_{C_l}} \right] K_b \quad (6)$$

Where  $\Delta C_{l,0}$  is the lift increment at zero angle of attack for the airfoil,  $C_{L\alpha}$  and  $C_{l\alpha}$  are respectively the lift curve slopes of the wing and the airfoil,  $\frac{(\alpha_{\delta})_{C_L}}{(\alpha_{\delta})_{C_l}} = K_c$  is the ratio of the three-dimensional flap effectiveness parameter to the two dimensional flap effectiveness one that can be plotted as the graph below:

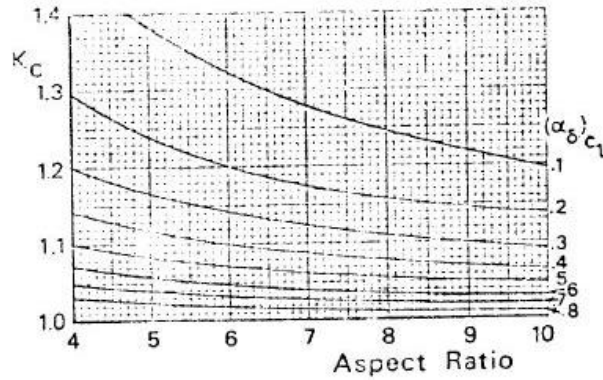
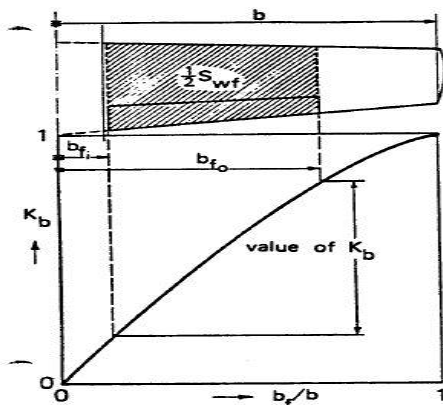


Figure 22:  $K_c$  variation with AR and  $(\alpha_{\delta})_{C_l}$

Finally  $K_b$ , a function of the flap span-wise extension, is a flap span effectiveness factor defined as follows:



$$K_b = \frac{\Delta C_{L,0} \text{ (partial span)}}{\Delta C_{L,0} \text{ (full span)}} \quad (7)$$

## 3.2 Variation of maximum lift coefficient

### 3.2.1 Determination of $\Delta C_{l,max}$ for the airfoil due to T. E. devices

An empirical method for predicting airfoil maximum lift increments for plain, split, and slotted flaps is presented in DATCOM. The maximum lift increment provided to an airfoil by the deflection of a trailing edge flap is given by:

$$\Delta C_{l,max} = k_1 k_2 k_3 (\Delta C_{l,max})_{base} \quad (8)$$

Where  $(\Delta C_{l,max})_{base}$  is the section maximum lift increment for 25 percent-chord flaps at the reference flap-deflection angle. The quantity  $k_1$  is a factor accounting for flap-chord-to-airfoil chord ratios,  $cf/c$ . The quantity  $k_2$  is a factor accounting for flap deflections. Finally,  $k_3$  is a factor accounting for flap motion as a function of flap deflection.

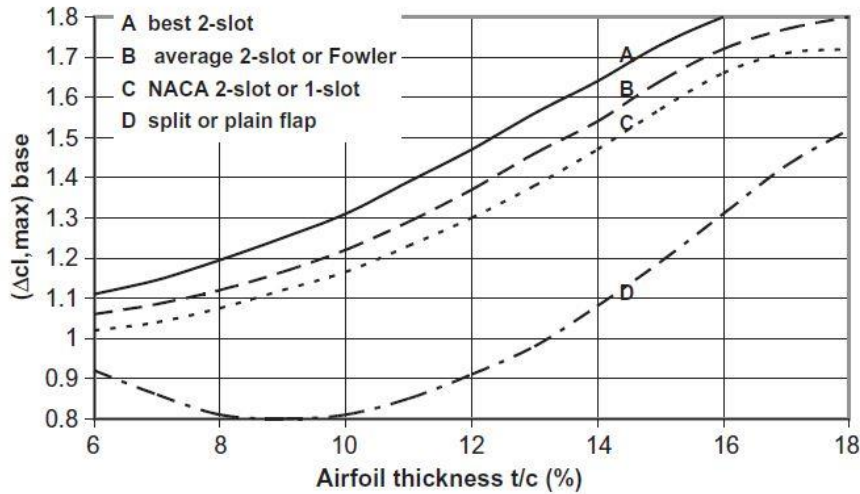


Figure 23: base maximum lift increments for 25% chord trailing edge flaps of various types at the reference flap angle. Curve A is for best 2-slot flaps with NACA airfoils, B is for 2-slot flaps with NACA airfoils or Fowler flaps with any airfoil, C is for NACA 2-slot flaps with NACA 6-series airfoils or NACA 1-slot flaps with any airfoil, and D is for split and plain flaps with any airfoil.

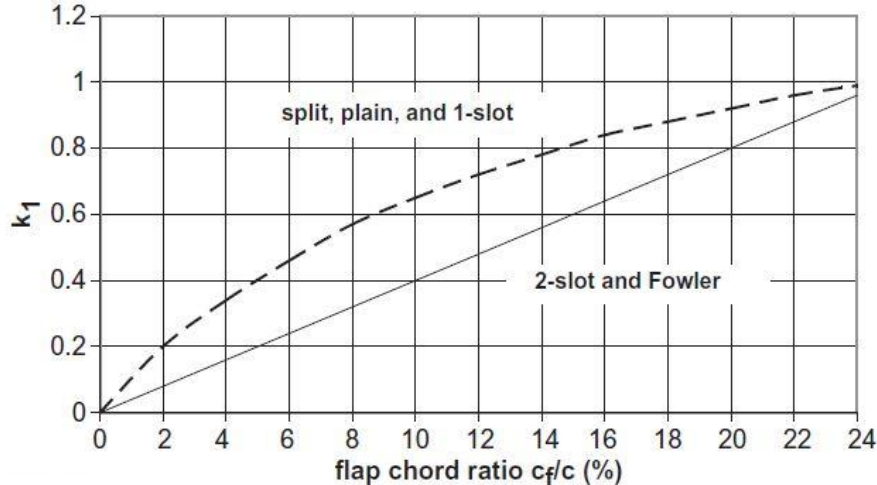


Figure 24:

Correction factor for trailing edge flap chord to airfoil-chord ratios,  $cf/c$ , other than 0.25.

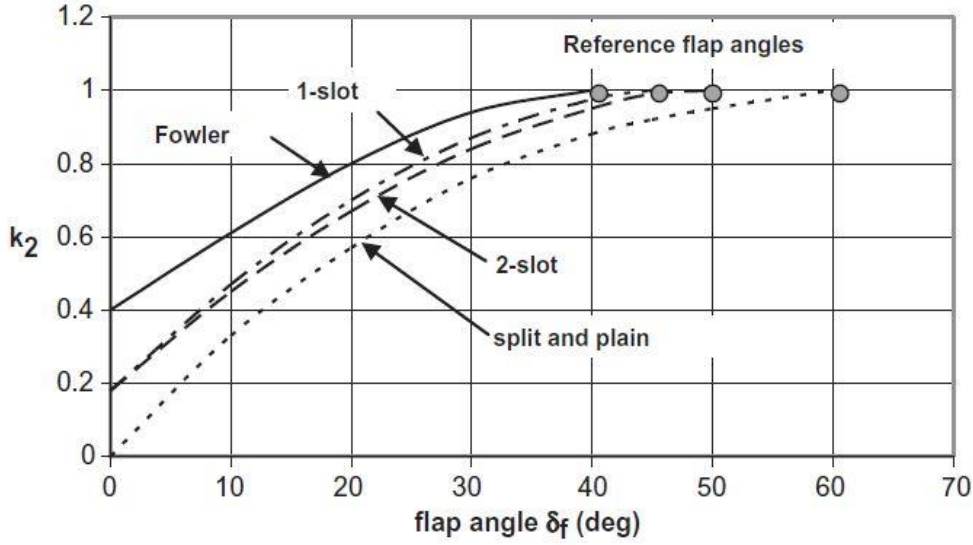


Figure 25: flap angle correction factor. The reference flap angle for each type of flap is shown as a solid symbol at  $k_2 = 1$ .

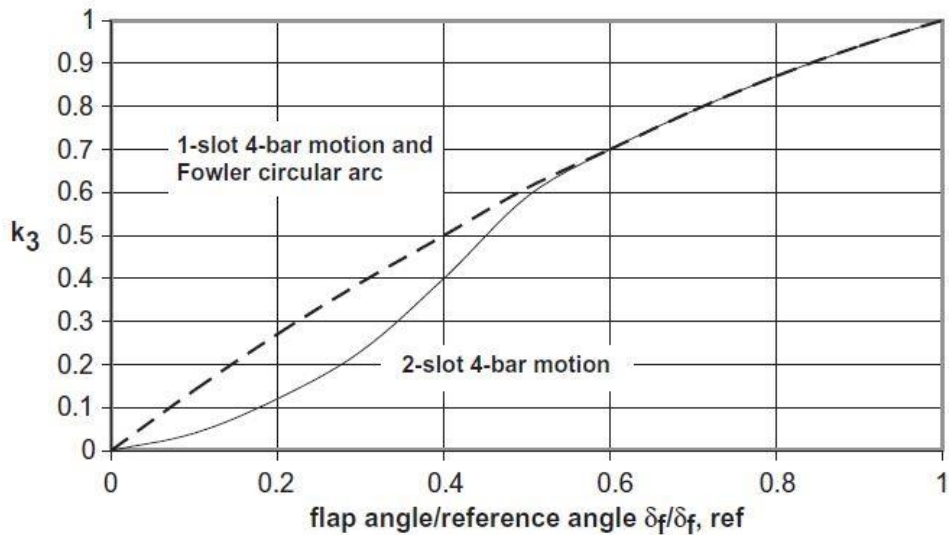


Figure 26: flap motion correction factor.

### 3.2.2 Determination of $\Delta C_{l, \max}$ for the airfoil due to L. E. devices

A method has been developed for predicting the stall of thin airfoils with leading edge flaps or slats. The DATCOM estimation method is based on the assumption that the flapped and unflapped airfoils stall when the respective pressure distributions about the noses are the same. The method gives best results for slat deflections less than  $20^\circ$  and slat chord-to-airfoil-chord ratios less than 0.20.

The effect of a leading edge flap or slat can be summarized in the delay of the leading edge separation to a higher angle of attack. Moreover, in this section only the increment of  $C_{l, \max}$  will be discussed, considering of no importance the effects on lift curve of inclination and  $C_{l_0}$ .

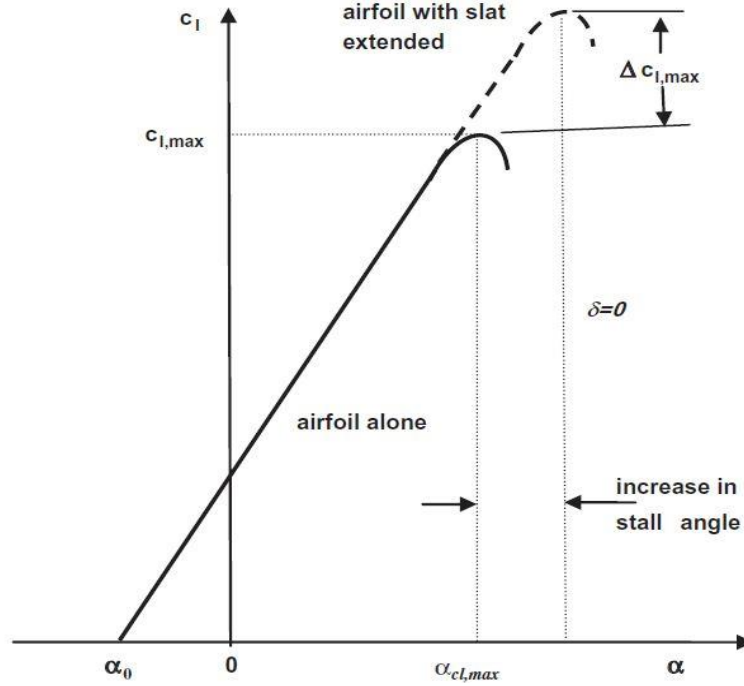


Figure 27: change in lift curve achieved by using a leading edge slat

The DATCOM method for leading edge flaps and slats proposes that the maximum lift increment for leading edge flaps or slats may be approximated by the following empirical relationship:

$$\Delta_{cl,max} = \left( \frac{\partial C_l}{\partial \delta} \right)_{max} \eta_{max} \eta_{\delta} \delta_s \frac{c'}{c} \quad (9)$$

The first term is the theoretical lift effectiveness which gives the rate of change of the lift coefficient with change in deflection angle; it is a function of the leading edge flap or slat chord to airfoil-chord ratio  $\frac{c_s}{c}$ . The second term,  $\eta_{max}$ , is an empirical factor which accounts for the effects of airfoil leading edge radius and maximum thickness. In the graph of this factor is presented the discontinuity in the curve for slats due to a lack of data. The third term,  $\eta_{\delta}$ , is another empirical factor which corrects for flap or slat deflections different from the optimum flap angle, it is a function of the flap or slot deflection angle  $\delta_s$ . The ratio  $\frac{c'}{c}$  accounts for the apparent increase in chord length when the slat is deflected and a slot is formed between the two airfoil elements.

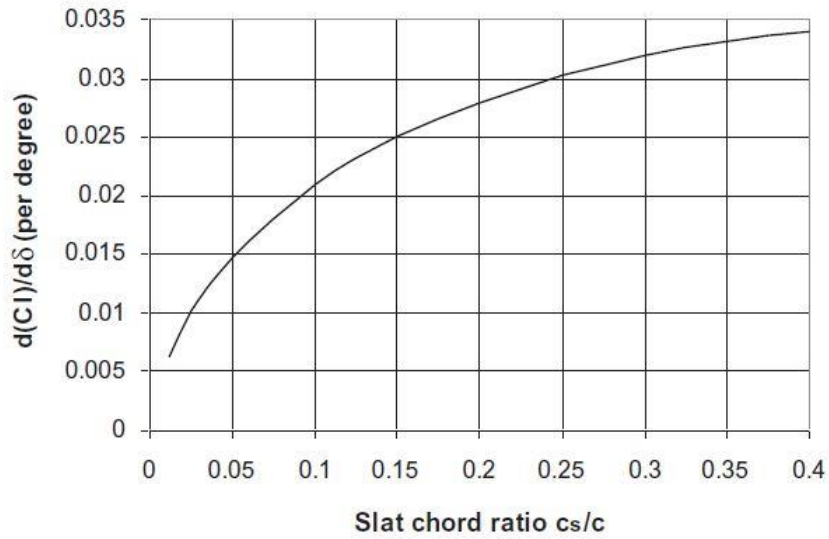


Figure 28: rate of change of airfoil lift coefficient with slat deflection (per degree)

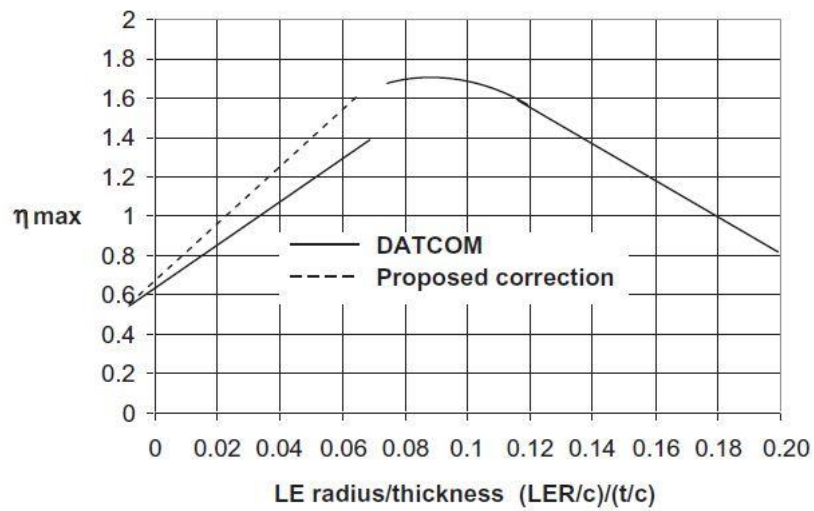


Figure 29: correction factor for leading edge radius and airfoil thickness ratio

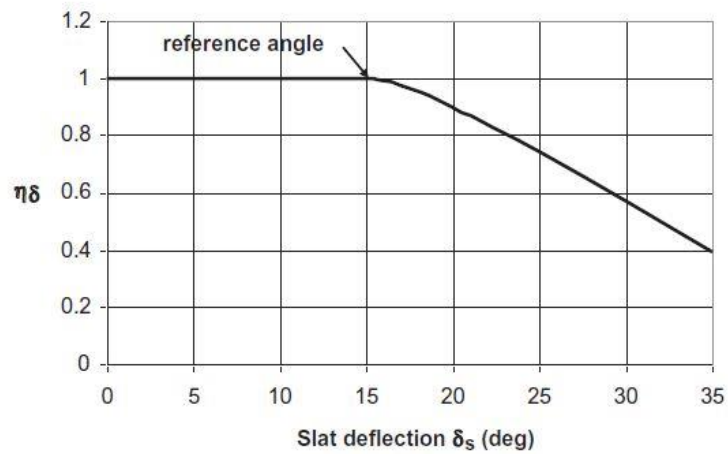


Figure 30: slat deflection correction factor as a function of deflection angle

### 3.2.3 Determination of $\Delta C_{L,max}$ for the wing due to T.E. devices

The increment in maximum lift coefficient for the wing due to the trailing edge flap deflection is given in the DATCOM method by the following equation:

$$\Delta C_{L,max,f} = \Delta C_{l,max} \frac{S_{wf}}{S} K_{\Lambda} \quad (10)$$

$\Delta C_{l,max}$  is the increment in lift coefficient due to flap deflection. The quantity  $\frac{S_{wf}}{S}$  is the ratio of wing area affected by the trailing edge flap deflection to the total wing area. The wing area affected by the flap may be written as:

$$S_{wf} = \left(\frac{b}{2}\right) c_r [2 - (1 - \lambda)(\eta_i - \eta_o)](\eta_i - \eta_o) \quad (11)$$

Where  $\lambda = \frac{c_t}{c_r}$  is the ratio of tip chord to the root chord,  $b$  is the wingspan,  $\eta_i$  is the inboard location of a flap while the outboard location is  $\eta_o$ .

The correction factor of sweepback is  $K_{\Lambda} = [1 - 0.08(\cos \Lambda_{c/4})^2](\cos \Lambda_{c/4})^{3/4}$  (12)

Finally, the lift coefficient for the wing with flaps deflected is:

$$C_{L,max,w} = C_{L,max} + \Delta C_{L,max,f} \quad (13)$$

### 3.2.4 Determination of $\Delta C_{L,max}$ for the wing due to L.E. devices

In the same way and using the same formulation of flaps, we express for slats:

$$\Delta C_{L,max,s} = \Delta C_{l,max} \frac{S_{ws}}{S} K_{\Lambda} \quad (14)$$

Then the maximum lift coefficient of the wing with a leading edge slat deflection is

$$C_{L,max,w} = C_{L,max} + \Delta C_{L,max,s} \quad (15)$$

In conclusion, for a wing, adding the effects of slats and flaps, we obtain the following expression for  $C_{L,max,w}$ :

$$C_{L,max,w} = C_{L,max} + \Delta C_{L,max,f} + \Delta C_{L,max,s} \quad (16)$$

### 3.3 Variation of lift gradient due to flap deflection

The lift gradient is affected by flap deflection in three ways:

- The chord extension increases  $C_{l\alpha}$ . This effect depends on the multiplicative factor  $\frac{c'}{c}$
- $C_{l\alpha}$  decreases not only with flap deflection, but also with the angle of attack, because  $\Delta C_l$  reduces with increasing  $\alpha$  due to the potential flow effect of flap deflection
- The effect of viscosity on the lift effectiveness of a flap increases with the angle of attack, thus reducing  $\Delta C_l$  with increasing  $\alpha$

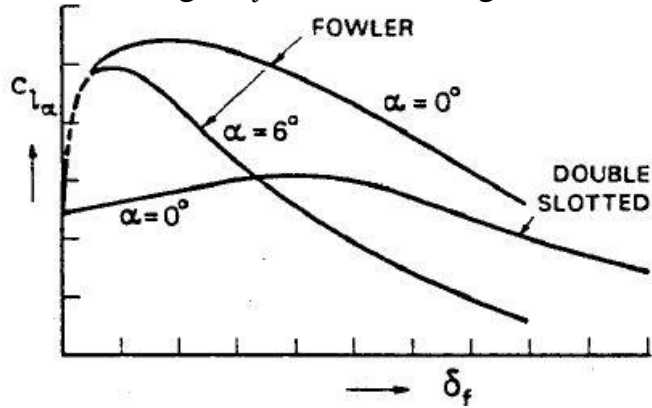


Figure 31: variation of lift gradient with flap deflection and angle of attack

The relationship written below approximates the results of the exact theory enough accurately and respects experimental data:

$$C_{l\alpha(\text{flaps down})} = C_{l\alpha(\text{flaps up})} \left( \frac{c'}{c} \left( 1 - \frac{c_f}{c'} (\sin \delta_f)^2 \right) \right) \quad (17)$$

The effect on wing may be estimated through the following formulation:

$$C_{L\alpha(\text{flaps down})} = C_{L\alpha(\text{flaps up})} \left\{ 1 + \frac{\Delta C_{L,0}}{\Delta C_{l,0}} \left[ \left( \frac{c'}{c} \left( 1 - \frac{c_f}{c'} (\sin \delta_f)^2 \right) - 1 \right) \right] \right\} \quad (18)$$

### 3.4 Variation of drag coefficient due to high-lift devices

There is also additional drag when the flaps are extended because of the larger wake produced in this condition. This is a boundary layer separation effect and occurs in addition to the induced drag accompanying the production of lift. A valid method to estimate the drag coefficient increment was presented by McCormick:

$$\Delta C_D = 0.9 \left( \frac{c_f}{c} \right)^{1.38} \left( \frac{s_{w,f}}{s} \right) (\sin \delta_f)^2 \quad (19)$$

For plain or split flaps the coefficient 0.9 is increased to 1.7.

As regard slats, there is no appreciable rate to drag.



## 4 Application on general-aviation aircrafts

A program in **Matlab** has been developed to study the effects of using high-lift devices on two types of aircraft wings in take-off and landing conditions.

In the main script, the user has to insert as input: geometry and aerodynamic data for wing, aerodynamic data for airfoil and geometric data for the chosen type of flap and slat.

The aim of the program is to give as aerodynamic output the modified parameters due to the use of high-lift systems, particularly the variation of lift curve and drag curve.

Before structuring the program, a preliminary work has been made: each graph shown in the methods described previously has been digitalized through the program **Get data graph digitizer** and all data collected have been interpolated by a special script generated by Matlab in order to be used in occurrence through functions.

The program has been realized to be adapted to lots of aircrafts, varying geometric and aerodynamic parameters and type and number of high-lift devices.

The computations presented, are valid for a Boeing 737 and an Atr 42.

See the *Appendix A* to view the full program structure.

The program is able to realize a plan view of the wing, showing the position and dimension of high-lift systems once inserted geometrical parameter:

$b$  is the wing-span

$c_1$  is the root chord at the station  $y=0$ ;

$c_2$  is the chord at a generic station  $0 < y < b/2$ ;

$c_3$  is the tip chord at the station  $y=b/2$ ;

$\Lambda_{LE}$  is the sweepback angle at the leading edge;

$\eta_i$  and  $\eta_o$  are respectively the beginning and ending station for the generic high-lift device, dimensionless than the half-opened wing;

$cf$  is the mean chord of a flap;

$cs$  is the mean chord of a slat.

See the *Appendix B* to have more information about the plan view program structure

## 4.1 Boeing 737

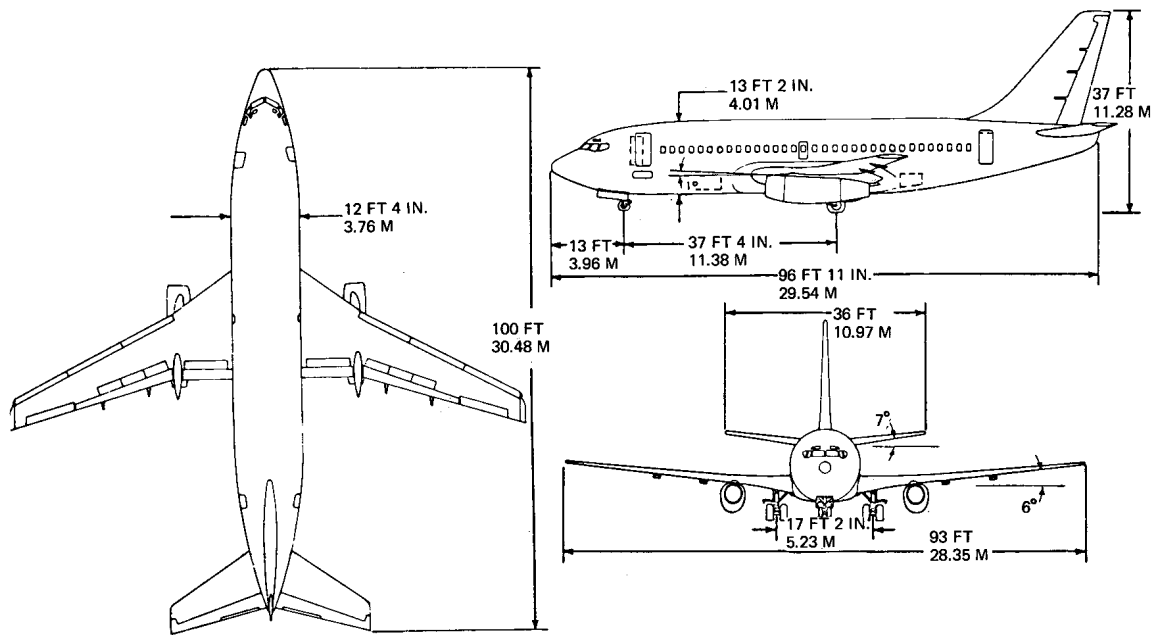


Figure 32: Boeing 737 plan view

The Boeing 737 is the most used aircraft in general aviation and is equipped of two double-slotted flaps, whose typical total deflections during take-off are about  $20^\circ$ , and during landing are about  $50^\circ$ .

As regard leading edge devices, when double slotted flaps are present at trailing edge, typical deflections are:  $20^\circ$  during take-off and  $35^\circ$  during landing.

The program will plot the trend of the curves both in clean configuration and flapped and slatted ones, from the input inserted, moreover the plan view is:

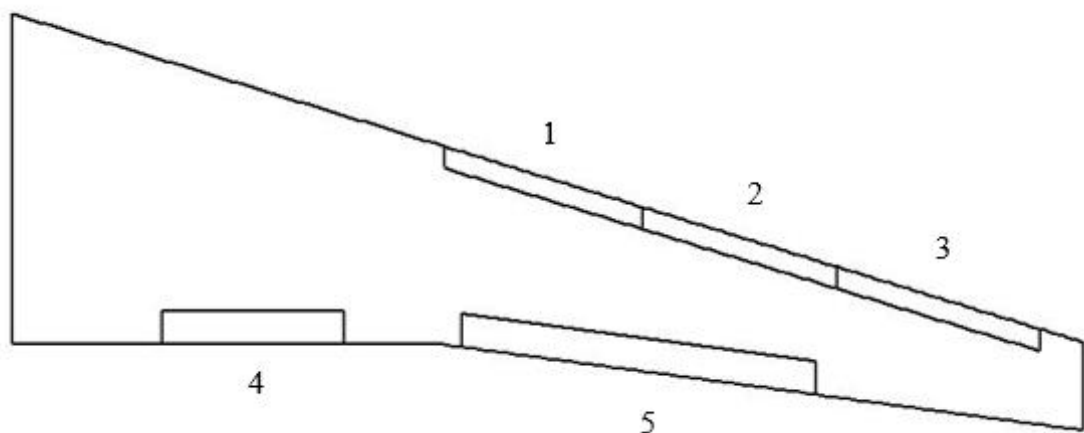


Figure 33: 1-2-3, Krueger flaps; 4-5, Double slotted flaps

The noteworthy output results for flapped and slatted configuration are:

- $C_{L-max}$
- $C_{L0}$
- $C_{L\alpha}$

**The geometric and aerodynamic parameter used for computations are:**

#### Input geometric data for wing

c1=8.33	root chord (1st station--> y=0)
c2=5	chord at second station (--> y=bg)
c3=2.22	tip chord (3rd station --> Y=b/2)
b=35.8	wing span
bg=7.22	second station
CD0=0.023	parasitic drag coefficient
t=0.74	thickness
e=0.80	Oswald factor
Lambda_Le=24.8	sweepback angle at leading edge (1st part of the wing)
Lambda_Le2=24.8	sweepback angle at leading edge (2nd part of the wing)

#### Input data for flap 1

type_flap	double slotted flap
deltaf1=15	first deflection
deltaf2=5	second deflection
deltaf3=0	third deflection
cf/c=0.1567	flap chord to mean wing chord ratio
deltaf_ref=50	deflection reference
ni=0.14	flap inboard
no=0.31	flap outboard

#### Input data for flap 2

type_flap_2=2	double slotted flap
deltaf1_2=15	first deflection
deltaf2_2=5	second deflection
deltaf3_2=0	third deflection
cf2/c=0.1567	flap chord to mean wing chord ratio
deltaf_ref_2=50	deflection reference
ni2=0.42	flap inboard
no2=0.75	flap outboard

#### Input data for slat 1

Delta_s=20	slat deflection
cs/c=0.1044	slat chord to mean wing chord ratio
c_ext_suC=1.1	extended chord to airfoil chord ratio
Le_radius=0.0097	Leading edge radius
ni_s=0.403	slat inboard
no_s=0.589	slat outboard

#### Input data for slat 2

Delta_s_2=20	slat deflection
cs2/c=0.1044	slat chord to mean wing chord ratio
c_ext_suC_2=1.1	extended chord to airfoil chord ratio
Le_radius_2=0.0097	Leading edge radius
ni2=0.589	slat inboard
no2=0.77	slat outboard

#### Input data for slat 3

Delta_s_3=20	slat deflection
cs3/c=0.1044	slat chord to mean wing chord ratio
c_ext_suC_3=1.1	extended chord to airfoil chord ratio
Le_radius_3=0.0097	Leading edge radius
ni3=0.77	slat inboard
no3=0.96	slat outboard

### 4.1.1 Graphical and numerical results for take-off computations

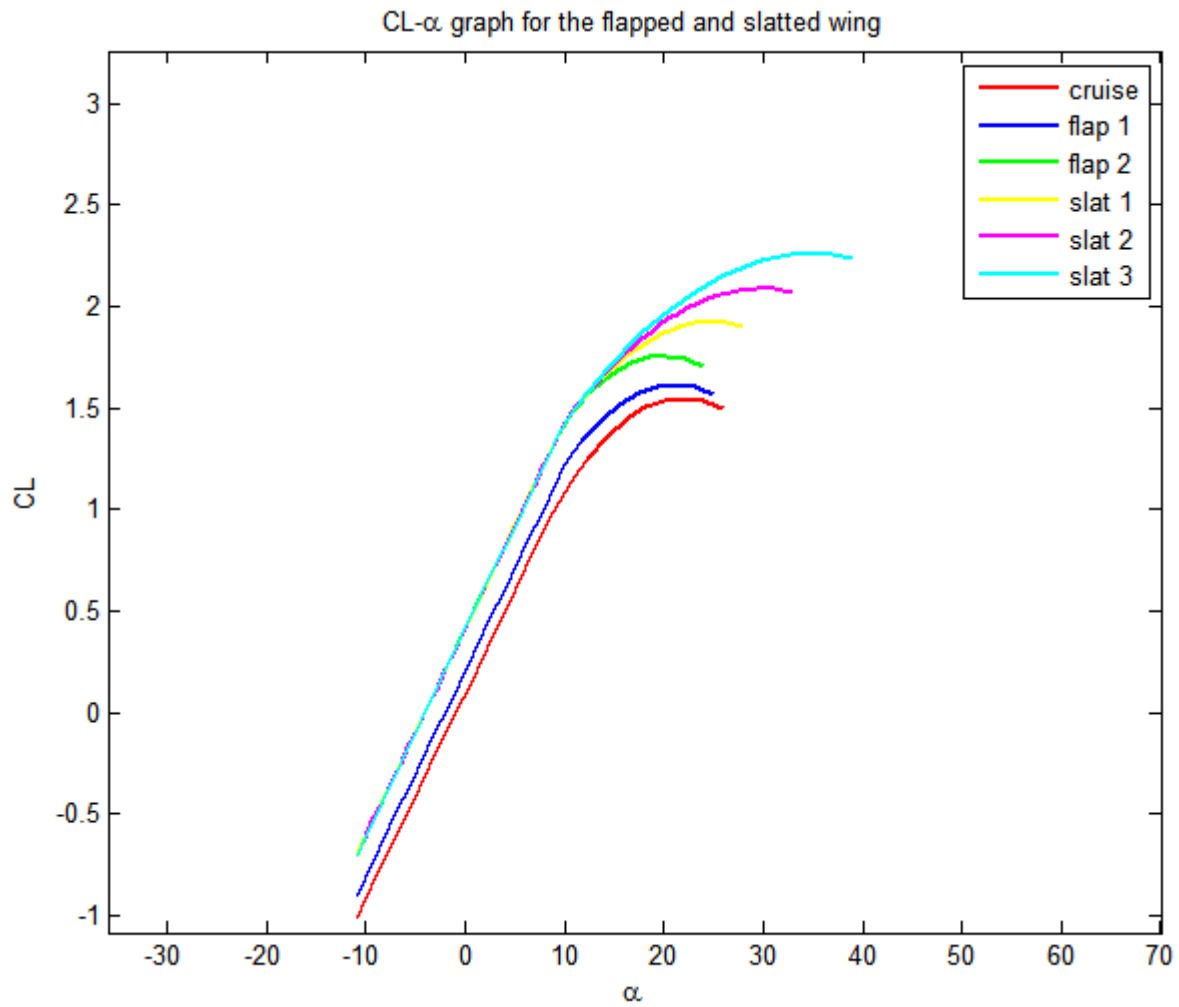


Figure 34

In the table for take-off below, final results are reported: there is an increase of  $C_{L_{max}}$ ,  $C_{L_0}$ ,  $C_{L_\alpha}$  and  $C_{D_0}$  as regard each flap, moreover there is only an increase of  $C_{L_{max}}$  as regard each slat.

	$\Delta C_{L_{max}}$	$\Delta C_{L_0}$	$\Delta C_{L_\alpha}$	$\Delta C_{D_0}$
<b>Flap 1</b>	0.0678	0.111	0.000272	0.002265
<b>Flap 2</b>	0.1387	0.20574	0.00055	0.004631
<b>Slat 1</b>	0.1676	0	0	0
<b>Slat 2</b>	0.1628	0	0	0
<b>Slat 3</b>	0.1714	0	0	0

Final effects:

$$C_{L_{max,w}}=2.258$$

$$C_{L_0,w}=0.4167$$

$$C_{L_\alpha,w}=0.1017$$

$$C_{D_0}=0.0299$$

### 4.1.2 Graphical and numerical results for landing computations

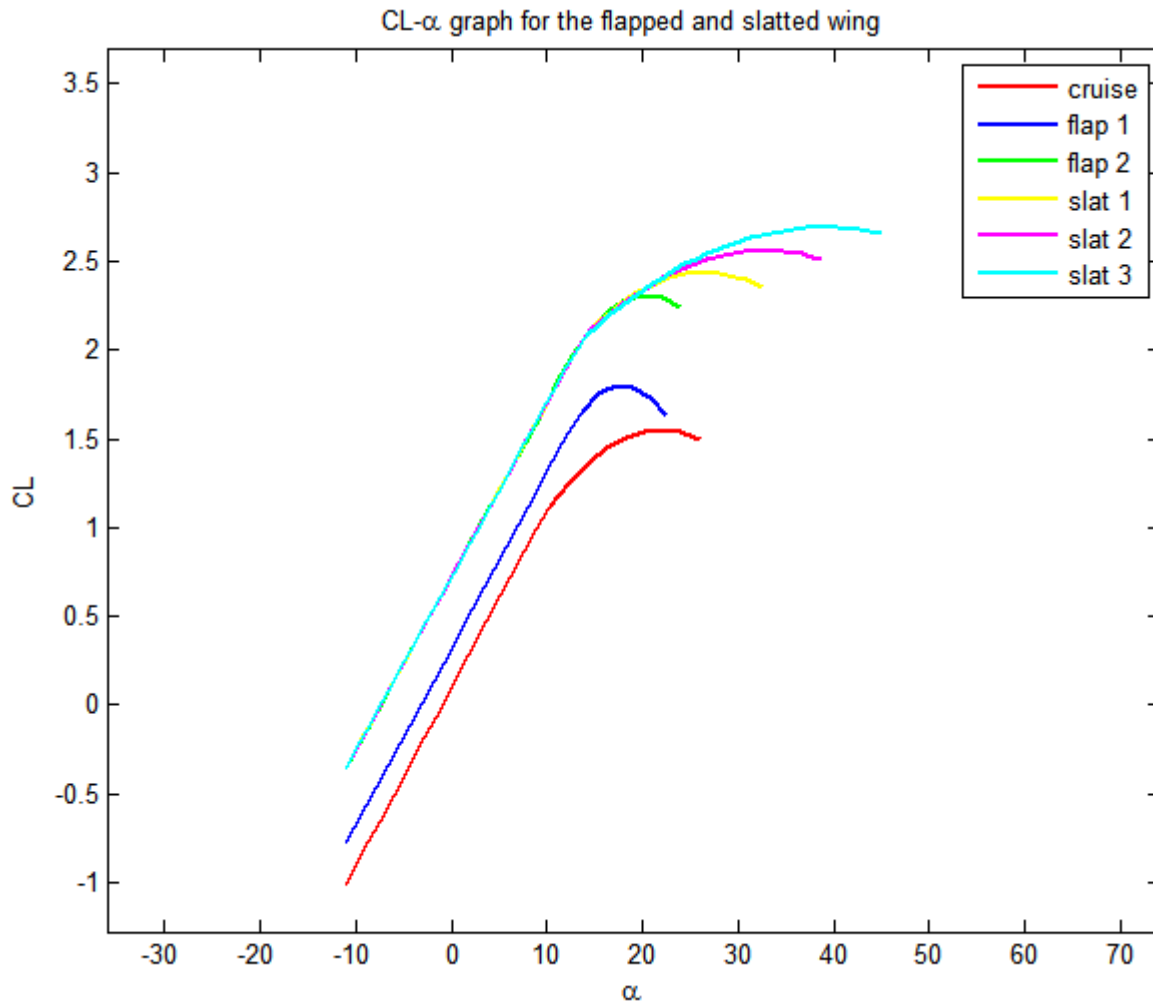


Figure 35

In the table for landing below, final results are reported: there is an increase of  $C_{L_{max}}$ ,  $C_{L_0}$ ,  $C_{L_\alpha}$  and  $C_{D_0}$  as regard each flap, moreover there is only an increase of  $C_{L_{max}}$  as regard each slat.

	$\Delta C_{L_{max}}$	$\Delta C_{L_0}$	$\Delta C_{L_\alpha}$	$\Delta C_{D_0}$
<b>Flap 1</b>	0.25	0.2178	-0.000991	0.011365
<b>Flap 2</b>	0.51	0.4038	-0.002	0.0232
<b>Slat 1</b>	0.1271	0	0	0
<b>Slat 2</b>	0.1235	0	0	0
<b>Slat 3</b>	0.13	0	0	0

Final effects:

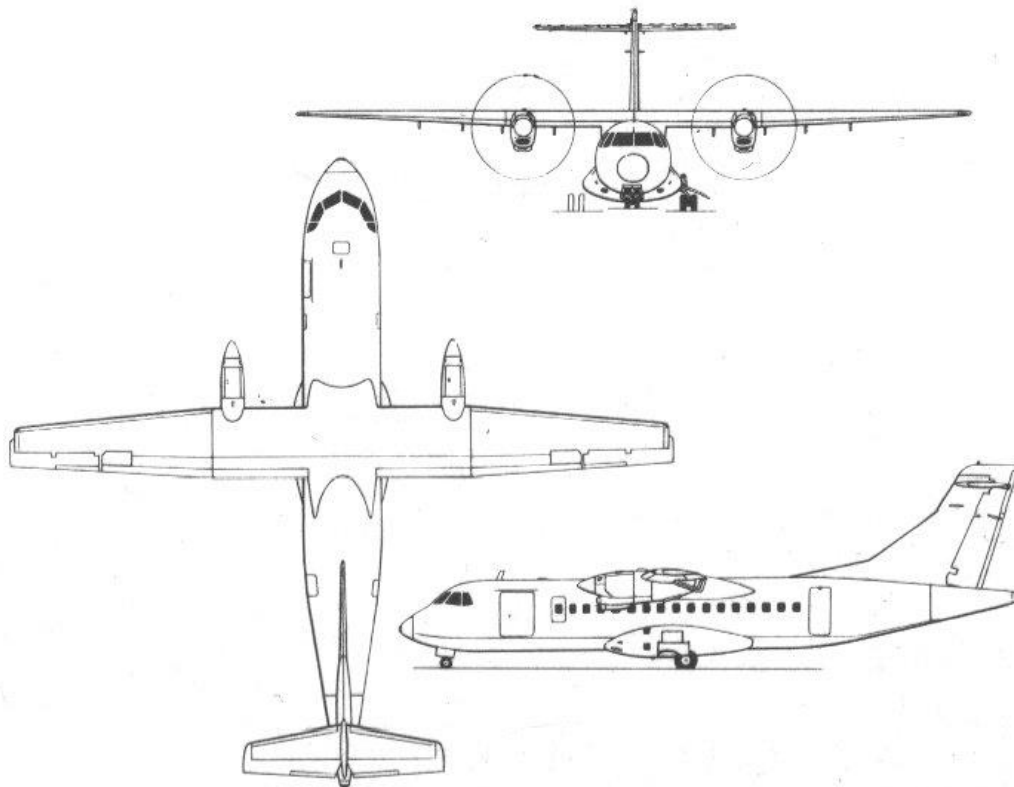
$$C_{L_{max,w}}=2.692$$

$$C_{L_0,w}=0.7216$$

$$C_{L_\alpha,w}=0.0979$$

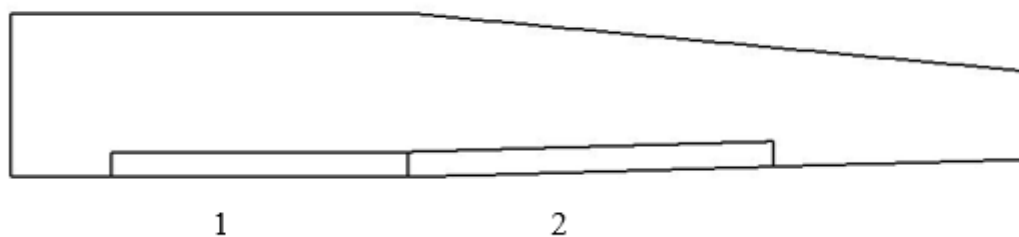
$$C_{D_0}=0.0576$$

## 4.2 ATR 42



The ATR 42 is a general aviation aircraft and is equipped of two single-slotted flaps, whose typical deflections during take-off are about  $20^\circ$ , and during landing are about  $40^\circ$ . ATR 42 is not equipped of leading edge devices.

The program will plot the trend of the curves both in clean configuration and flapped ones, from the input inserted. The plan view is:



*ATR 42: 1-2, single slotted flaps*

The noteworthy output results for flapped configuration are:

- $C_{L-max}$
- $C_{L0}$
- $C_{L\alpha}$

**The geometric and aerodynamic parameter used for computations are:**

#### Input geometric data for wing

<code>c1=2.6</code>	root chord (1st station--> $y=0$ )
<code>c2=c1</code>	chord at second station (--> $y=b_g$ )
<code>c3=1.4</code>	tip chord (3rd station --> $Y=b/2$ )
<code>b=24.57</code>	wing span
<code>b_g=4.80</code>	second station
<code>CD0=0.03</code>	parasitic drag coefficient
<code>t=0.3</code>	thickness
<code>e=0.80</code>	Oswald factor
<code>Lambda_Le=0</code>	sweepback angle at leading edge (1st part of the wing)
<code>Lambda_Le2=7</code>	sweepback angle at leading edge (1st part of the wing)

#### Input data for flap 1

<code>type_flap</code>	single slotted flap
<code>cf/c=0.1711</code>	flap chord to mean wing chord ratio
<code>deltaf=20</code>	flap deflection
<code>deltaf_ref=45</code>	reference angle
<code>ni=0.098</code>	flap inboard
<code>no=b_g/(b/2)</code>	flap outboard

#### Input data for flap 2

<code>type_flap_2</code>	single slotted flap
<code>cf2/c=0.1711</code>	flap chord to mean wing chord ratio
<code>deltaf_2=20</code>	flap deflection
<code>deltaf_ref_2=45</code>	reference angle
<code>ni2=no</code>	flap inboard
<code>no2=0.75</code>	flap outboard

### 4.2.1 Graphical and numerical results for take-off computations

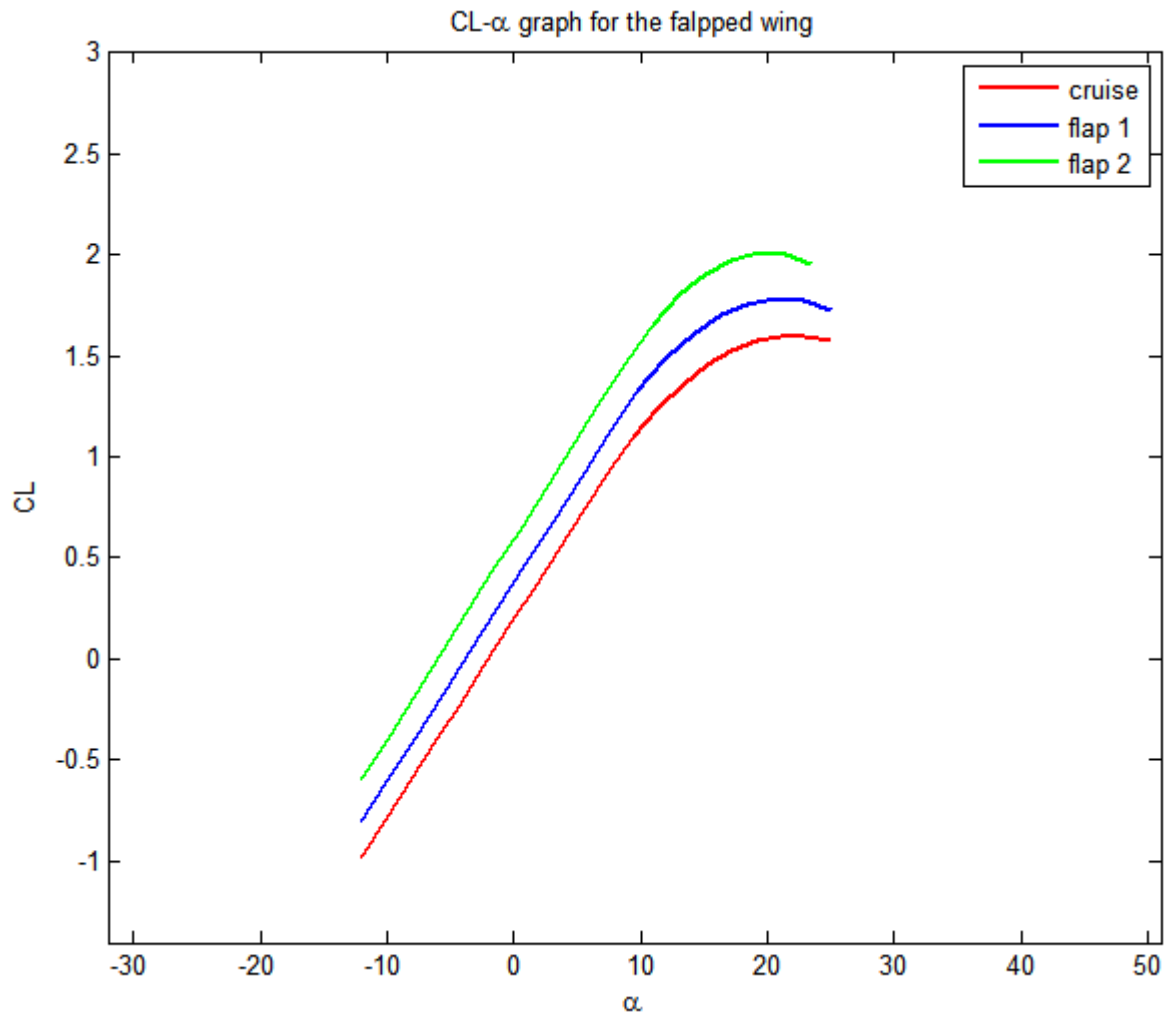


Figure 36

In the table for take-off below, final results are reported: there is an increase of  $C_{L_{max}}$ ,  $C_{L_0}$ ,  $C_{L_\alpha}$  and  $C_{D0}$  as regard each flap.

	$\Delta C_{L_{max}}$	$\Delta C_{L_0}$	$\Delta C_{L_\alpha}$	$\Delta C_{D0}$
<b>Flap 1</b>	0.1822	0.18023	0.00047	0.00399
<b>Flap 2</b>	0.2273	0.21891	0.00059	0.00498

Final effects:

$$C_{L_{max,w}}=2.01$$

$$C_{L_0,w}=0.595$$

$$C_{L_\alpha,w}=0.0991$$

$$C_{D0}=0.0389$$



## 4.2.2 Graphical and numerical results for landing computations

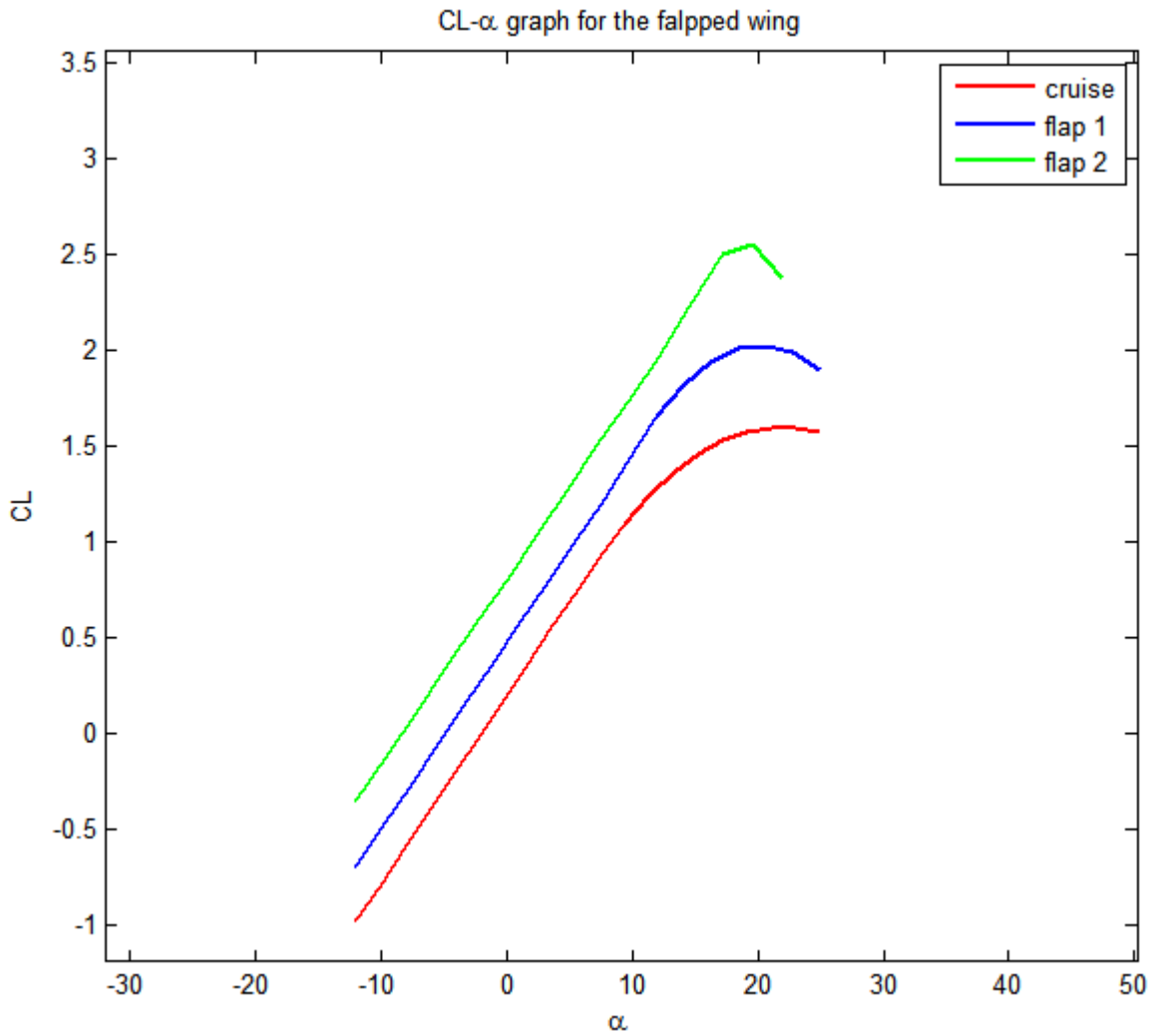


Figure 37

In the table for landing below, final results are reported: there is an increase of  $C_{L_{max}}$ ,  $C_{L_0}$ ,  $C_{L_\alpha}$  and  $C_{D_0}$  as regard each flap.

	$\Delta C_{L_{max}}$	$\Delta C_{L_0}$	$\Delta C_{L_\alpha}$	$\Delta C_{D_0}$
<b>Flap 1</b>	0.4277	0.27452	-0.000744	0.014114
<b>Flap 2</b>	0.5338	0.33343	-0.000929	0.017614

Final effects:

$$C_{L_{max,w}}=2.561$$

$$C_{L_0,w}=0.8039$$

$$C_{L_\alpha,w}=0.0963$$

$$C_{D_0}=0.061$$

## Appendix A

```
%Script for variation of CL and CD in clean configuration due to high-lift
systems

%How to use the program
%The user has to insert all input data for wing, all flaps and slats;
%All angles are entered in degrees;
%It's possible to insert the type of flap for computations.
%The parameter 'type_flap' can assume six different values:
%1) type_flap=1 ---> Single slotted flap
%2) type_flap=2 ---> Double slotted flap
%3) type_flap=3 ---> Split flap
%4) type_flap=4 ---> Plain flap
%5) type_flap=5 ---> Fowler flap
%6) type_flap=6 ---> Triple slotted flap

%According to the theory adopted, for all kind of leading edge devices (slats
%and Krueger flaps), computations are the same.

%Input geometric data for wing
c1=8.33; %root chord (1st station--> y=0)
c2=5; %chord at second station (--> y=b/2)
c3=2.22; %tip chord (3rd station --> Y=b/2)
b=35.8; %wing span
bg=7.22; %second station
CD0=0.023; %parasitic drag coefficient
t=0.74; %thickness
e=0.80; %Oswald factor

Lambda_Le=24.8; %sweepback angle at leading edge (1st part of the wing)
Lambda_Le=Lambda_Le*pi/180;
Lambda_Le2=24.8; %sweepback angle at leading edge (2nd part of the wing)
%%
%Equivalent wing data
S1=(c1+c2)*bg; S2=(c2+c3)*((b/2)-bg);
ct=c3; %tip chord
cr=(S1+S2)/((b/2)-ct); %root chord

%Input aerodynamic data for airfoil
Cl_alpha=0.11; %curve slope
Cl0=0.25; %Cl at alpha zero lift
Cl_max=1.8; %max value of Cl
alpha_star=11; %angle of attack at the end of linearity
alpha0=-2.3; %angle of attack at zero lift

%%

%Input aerodynamic data for wing
CL_alpha=0.1009;
CL0=0.1;
CL_max=1.55;
Alpha_star=11;
Alpha0=-1;

%Input data for flap 1
```

```

type_flap=2;
deltaf1=15; %first deflection
deltaf1=deltaf1*pi/180;
deltaf2=5; %second deflection
deltaf2=deltaf2*pi/180;
deltaf3=0; %third deflection
deltaf3=deltaf3*pi/180;
cf=0.833; %mean flap chord
deltaf=deltaf1+deltaf2+deltaf3; %flap deflection
deltaf_ref=50; %deflection reference
deltaf_ref=deltaf_ref*pi/180;
ni=0.14; %flap inboard
no=0.31; %flap outboard

%Input data for flap 2
type_flap_2=2;
deltaf1_2=15;
deltaf1_2=deltaf1_2*pi/180;
deltaf2_2=5;
deltaf2_2=deltaf2_2*pi/180;
deltaf3_2=0;
deltaf3_2=deltaf3_2*pi/180;
cf2=0.833;
deltaf_2=deltaf1_2+deltaf2_2+deltaf3_2;
deltaf_ref_2=50;
deltaf_ref_2=deltaf_ref_2*pi/180;
ni2=0.42;
no2=0.75;

%Input data for slat 1
Delta_s=20; %slat deflection
Delta_s=Delta_s*pi/180;
cs=0.555; %slat chord
c_ext_suC=1.1; %extended chord to airfoil chord ratio
Le_radius=0.0097; %Leading edge radius
ni_s=0.403; %slat inboard
no_s=0.589; %slat outboard

%Input data for slat 2
Delta_s_2=20; %slat deflection
Delta_s_2=Delta_s_2*pi/180;
cs2=0.555; %slat chord
c_ext_suC_2=1.1; %extended chord to airfoil chord ratio
Le_radius_2=0.0097; %Leading edge radius
nis2=0.589; %slat inboard
nos2=0.77; %slat outboard

%Input data for slat 3
Delta_s_3=20; %slat deflection
Delta_s_3=Delta_s_3*pi/180;
cs3=0.555; %slat chord
c_ext_suC_3=1.1; %extended chord to airfoil chord ratio
Le_radius_3=0.0097; %Leading edge radius
nis3=0.77; %slat inboard
nos3=0.96; %slat outboard
%Input data for slat 4
Delta_s_4=0; %slat deflection
Delta_s_4=Delta_s_4*pi/180;
cs4=0; %slat chord
c_ext_suC_4=0; %extended chord to airfoil chord ratio
Le_radius_4=0; %Leading edge radius

```

```

nis4=0; %slat inboard
nos4=0; %slat outboard

%Output geometric data (wing)
S=((cr+ct)*(b/2)); %wing surface
AR=(b^2)/S; %Aspect Ratio
lambda=ct/cr;
c=2/3*cr*(1+lambda+lambda^2)/(1+lambda); %mean aerodynamic chord
TsuC=t/c;
CfsuC=cf/c;
lambda_cquarti=tan(Lambda_Le)-((1-lambda)/(AR*(1+lambda)));

%%

%Output data for flap1
Swf=abs(b/2*cr*(2-(1-lambda)*(ni-no))*(ni-no));%wing surface where flap is
located
bf=(no-ni)*b/2;
Delta_alpha_max_1=Delta_alpha_max(deltaf);%variation of stall-angle due to flap
deflection
%Output data for flap 2
Swf_2=abs(b/2*cr*(2-(1-lambda)*(ni2-no2))*(ni2-no2));%wing surface where flap is
located
bf_2=(no2-ni2)*b/2;
Delta_alpha_max_2=Delta_alpha_max(deltaf_2);
%Output data for slat 1
CSsuC=cs/c;
Le_radius_su_TsuC=Le_radius/TsuC;%Leading edge radius
Sws=abs(b/2*cr*(2-(1-lambda)*(ni_s-no_s))*(ni_s-no_s));%wing surface where slat
is located
Delta_alpha_max_s1=Delta_alpha_max(Delta_s);
%Output data for slat 2
CSsuC_2=cs2/c;
Le_radius_su_TsuC_2=Le_radius_2/TsuC;%Leading edge radius
Sws_2=abs(b/2*cr*(2-(1-lambda)*(nis2-nos2))*(nis2-nos2));%wing surface where
slat is located
Delta_alpha_max_s2=Delta_alpha_max(Delta_s_2);
%Output data for slat 3
CSsuC_3=cs3/c;
Le_radius_su_TsuC_3=Le_radius_3/TsuC;%Leading edge radius
Sws_3=abs(b/2*cr*(2-(1-lambda)*(nis3-nos3))*(nis3-nos3));%wing surface where
slat is located
Delta_alpha_max_s3=Delta_alpha_max(Delta_s_3);
%Output data for slat 4
CSsuC_4=cs4/c;
Le_radius_su_TsuC_4=Le_radius_4/TsuC;%Leading edge radius
Sws_4=abs(b/2*cr*(2-(1-lambda)*(nis4-nos4))*(nis4-nos4));%wing surface where
slat is located
Delta_alpha_max_s4=Delta_alpha_max(Delta_s_4);

%Wing design
figure(1)
Wing_design(Lambda_Le,Lambda_Le2,b,c1,c2,c3,bg,cf,ni,no,cf2,ni2,no2,cs,ni_s,no_s
,cs2,nis2,nos2,cs3,nis3,nos3,cs4,nis4,nos4);

%Flap 1 effects

%Variation of airfoil parameters (2D)

```

```

%Determination of Delta_Clmax:
k1=kappal(type_flap,cf/c);
k2=kappa2(type_flap,deltaf);
k3=kappa3(type_flap,deltaf/deltaf_ref);
Delta_Clmax_base=Delta_Cl_maxbase(type_flap,t/c);
Delta_Clmax=k1*k2*k3*(Delta_Clmax_base);

%Determination of delta_CL0:
thetaf=acos(2*(cf/c)-1);
alphadelta = 1-(thetaf-sin(thetaf))/pi; %rate of change of zero lift angle of
attack due to flap deflection.
etadelta=eta_delta_flap(type_flap,deltaf);
delta_CL0=etadelta*alphadelta*Cl_alpha*deltaf*180/pi;
%Calculation of the extended chord for flap:
dCsuCf=deltaC_su_Cf(type_flap,deltaf);
c_ext=c*(1+dCsuCf*cf/c);
%Parameter variation due to flap:
Cl_alpha1=Cl_alpha*(c_ext/c*(1-cf/c_ext*(sin(deltaf))^2));
Cl_max1=Cl_max+Delta_Clmax;
CL01=CL0+delta_CL0;

%Variation of wing parameters (3D)

%Variation of CL0:

Kc=kappac(alphadelta,AR);
Kb=kb2(bf/b);
delta_CL0=delta_CL0*Cl_alpha/CL_alpha*Kc*Kb;

CL01=CL0+delta_CL0;

%Variation of CL_max:
K_lambda=(1-0.08*(cos(lambda_cquarti))^2)*(cos(lambda_cquarti))^(3/4);
Delta_CLmax=Delta_Clmax*Swf/S*K_lambda;

CL_max1=CL_max+Delta_CLmax;
%Slope variation
CL_alpha1=CL_alpha*(1+(Delta_CLmax/Delta_Clmax)*((c_ext/c*(1-cf/c_ext*(sin(deltaf))^2))-1));

%%
%Flap 2 effects

%Variation of airfoil parameters (2D)
%Determination of Delta_Clmax:
k1_2=kappal(type_flap_2,cf2/c);
k2_2=kappa2(type_flap_2,deltaf_2);
k3_2=kappa3(type_flap_2,deltaf_2/deltaf_ref_2);
Delta_Clmax_base_2=Delta_Cl_maxbase(type_flap_2,t/c);
Delta_Clmax_2=k1_2*k2_2*k3_2*(Delta_Clmax_base_2);

%Determination of delta_CL0:
thetaf_2=acos(2*(cf2/c)-1);
alphadelta_2 = 1-(thetaf_2-sin(thetaf_2))/pi;%rate of change of zero lift angle
of attack due to flap deflection.
etadelta_2=eta_delta_flap(type_flap_2,deltaf_2);

```

```

delta_CL0_2=etadelta_2*alphadelta_2*Cl_alpha*deltaf_2*180/pi;
%Calculation of the extended chord for flap:
dCsuCf_2=deltaC_su_Cf(type_flap_2,deltaf_2);
c_ext_2=c*(1+dCsuCf_2*cf2/c);
%Parameter variation due to flap:
Cl_alpha2=Cl_alpha*(c_ext_2/c*(1- cf2/c_ext_2*(sin(deltaf_2))^2));
Cl_max2=Cl_max+Delta_CLmax_2;
Cl02=Cl0+delta_CL0_2;

%Variation of wing parameters (3D)


%Variation of CL0:
Kc_2=kappac(alphadelta_2,AR);
Kb_2=kb2(bf_2/b);
delta_CL0_2=delta_CL0_2*Cl_alpha/CL_alpha*Kc_2*Kb_2;

CL02=CL0+delta_CL0_2;

%Variation of CL_max:
K_lambda=(1-0.08*(cos(lambda_cquarti))^2)*(cos(lambda_cquarti))^(3/4);
Delta_CLmax_2=Delta_CLmax_2*Swf_2/S*K_lambda;

CL_max2=CL_max+Delta_CLmax_2;
%Slope variation
CL_alpha2=CL_alpha*(1+(Delta_CLmax_2/Delta_CLmax_2)*((c_ext_2/c*(1- cf2/c_ext_2*(sin(deltaf_2))^2))-1));

%Slat 1
%Determination of airfoil parameters

eta_max_s=Datcom_corretto(Le_radius_su_TsuC);
etadelta_s=eta_delta(Delta_s);
dCl_su_dDelta_max=dCl(CSsuC);
Delta_CLmax_slat=dCl_su_dDelta_max*eta_max_s*etadelta_s*Delta_s*180/pi*c_ext_suC
;

Cl_max1_s=Cl_max+Delta_CLmax_slat;

%Determination of wing parameter
K_lambda=(1-0.08*(cos(lambda_cquarti))^2)*(cos(lambda_cquarti))^(3/4);
Delta_CLmax1_s=Delta_CLmax_slat*(Sws/S)*K_lambda;
CL_max1_s=CL_max+Delta_CLmax1_s;

%Slat 2
%Determination of airfoil parameters

eta_max_s_2=Datcom_corretto(Le_radius_su_TsuC_2);
etadelta_s_2=eta_delta(Delta_s_2);
dCl_su_dDelta_max_2=dCl(CSsuC_2);
Delta_CLmax_slat_2=dCl_su_dDelta_max_2*eta_max_s_2*etadelta_s_2*Delta_s_2*180/pi
*c_ext_suC_2;

Cl_max2_s=Cl_max+Delta_CLmax_slat_2;

%Determination of wing parameter

```

```

K_lambda=(1-0.08*(cos(lambda_cquarti))^2)*(cos(lambda_cquarti))^(3/4);
Delta_CLmax2_s=Delta_CLmax_slat_2*(Sws_2/S)*K_lambda;
CL_max2_s=CL_max+Delta_CLmax2_s;

%Slat 3
%Determination of airfoil parameters

eta_max_s_3=Datcom_corretto(Le_radius_su_TsuC_3);
etadelta_s_3=eta_delta(Delta_s_3);
dCl_su_dDelta_max_3=dCl(CSsuC_3);
Delta_CLmax_slat_3=dCl_su_dDelta_max_3*eta_max_s_3*etadelta_s_3*Delta_s_3*180/pi
*c_ext_suC_3;

CL_max3_s=CL_max+Delta_CLmax_slat_3;

%Determination of wing parameter
K_lambda=(1-0.08*(cos(lambda_cquarti))^2)*(cos(lambda_cquarti))^(3/4);
Delta_CLmax3_s=Delta_CLmax_slat_3*(Sws_3/S)*K_lambda;
CL_max3_s=CL_max+Delta_CLmax3_s;

%Slat 4
%Determination of airfoil parameters

eta_max_s_4=Datcom_corretto(Le_radius_su_TsuC_4);
etadelta_s_4=eta_delta(Delta_s_4);
dCl_su_dDelta_max_4=dCl(CSsuC_4);
Delta_CLmax_slat_4=dCl_su_dDelta_max_4*eta_max_s_4*etadelta_s_4*Delta_s_4*c_ext_
suC_4;

CL_max4_s=CL_max+Delta_CLmax_slat_4;

%Determination of wing parameter
K_lambda=(1-0.08*(cos(lambda_cquarti))^2)*(cos(lambda_cquarti))^(3/4);
Delta_CLmax4_s=Delta_CLmax_slat_4*(Sws_4/S)*K_lambda;
CL_max4_s=CL_max+Delta_CLmax4_s;

%Wing ultimate computations
CL_max_w_flap=CL_max+Delta_CLmax+Delta_CLmax_2;
CL_max_w=CL_max+Delta_CLmax+Delta_CLmax_2+Delta_CLmax1_s+Delta_CLmax2_s+Delta_CL
max3_s;
figure(2)
graficor(CL_alpha,CL_max, CL0, Alpha_star,Alpha0);hold on;
alpha_max_1=graficob(CL_alpha1,CL_max1,
CL01,Alpha_star,Alpha0,Delta_alpha_max_1,alpha_max);
alpha_max_2=graficove(CL_alpha1+CL_alpha2-CL_alpha,CL_max1+CL_max2-CL_max,
CL01+CL02-CL0,Alpha_star,Alpha0,Delta_alpha_max_2,alpha_max_1);
alpha_max_3=graficog_slat(CL_alpha1+CL_alpha2-
CL_alpha,CL_max1_s+CL_max1+CL_max2-2*CL_max,CL01+CL02-CL0,
Alpha_star,Alpha0,Delta_alpha_max_s1,alpha_max_2);
alpha_max_4=graficom_slat(CL_alpha1+CL_alpha2-
CL_alpha,CL_max1_s+CL_max2_s+CL_max1+CL_max2-3*CL_max,CL01+CL02-CL0,
Alpha_star,Alpha0,Delta_alpha_max_s2,alpha_max_3);
graficoc_slat(CL_alpha1+CL_alpha2-
CL_alpha,CL_max1_s+CL_max2_s+CL_max3_s+CL_max1+CL_max2-4*CL_max,CL01+CL02-CL0,
Alpha_star,Alpha0,Delta_alpha_max_s3,alpha_max_4);
legend('cruise','flap 1 ','flap 2 ','slat 1','slat 2 ','slat 3 ');
title('CL-\alpha graph for the flapped and slatted wing');

```

## Appendix B

```
function
disegno=Wing_design(freccia,freccia2,b,cr,cc,ct,bc,cf1,nif1,nof1,cf2,nif2,nof2,c
s1,nis1,nos1,cs2,nis2,nos2,cs3,nis3,nos3,cs4,nis4,nos4)

%Wing drawing:
nis1=nis1*b/2;
nis2=nis2*b/2;
nis3=nis3*b/2;
nis4=nis4*b/2;
nos1=nos1*b/2;
nos2=nos2*b/2;
nos3=nos3*b/2;
nos4=nos4*b/2;
nif1=nif1*b/2;
nif2=nif2*b/2;
nof1=nof1*b/2;
nof2=nof2*b/2;

if nof1<nif1
    error('ERROR: the correct input is ni<=no')
end
if nof2<nif2
    error('ERROR: the correct input is ni<=no')
end
if nos1<nis1
    error('ERROR: the correct input is ni<=no')
end
if nos2<nis2
    error('ERROR: the correct input is ni<=no')
end
if nos3<nis3
    error('ERROR: the correct input is ni<=no')
end
%The upper part of the wing:
N=100;

freccia=-freccia;
x=linspace(0,bc,N);
q=0; p=tan(freccia);
y=p*x+q;
figure(1)
plot(x,y,'k-','linewidth',2);
hold on;

x=linspace(bc,b/2,N);
y=(p*bc+q)+tan(-freccia2*pi/180)*(x-bc);
plot(x,y,'k-','linewidth',2);
hold on;

%root chord:

y=linspace(-cr,0,N);
p1=0;q1=0;
x=p1*y+q1;
plot(x,y,'k-','linewidth',2);
hold on;
%lower part of the wing, from 1st to 2nd station:
```



```

x=linspace(0,bc,N);
y=x/bc*((p*bc+q)-cc+cr)-cr;
plot(x,y,'k-','linewidth',2);
hold on;

%tip chord:
y=linspace((p*bc+q)+tan(-freccia2*pi/180)*(b/2-bc),((p*bc+q)+tan(-
freccia2*pi/180)*(b/2-bc))-ct,N);
p1=0; q1=b/2;
x=p1*y+q1;
plot(x,y,'k-','linewidth',2);
hold on;

%lower part of the wing, from 2nd to 3rd station:
x=linspace(bc,b/2,N);
y=(x-bc)/(b/2-bc)*(((p*bc+q)+tan(-freccia2*pi/180)*(b/2-bc))-((p*bc+q)+tan(-
freccia2*pi/180)*(bc-bc))+cc-ct)+((p*bc+q)+tan(-freccia2*pi/180)*(bc-bc))-cc;
plot(x,y,'k-','linewidth',2);
hold on;

%flap1:

%flap chord at nif:
y=linspace(nif1/bc*((p*bc+q)-cc+cr)-cr,nif1/bc*((p*bc+q)-cc+cr)-cr+cf1,N);
p1=0; q1=nif1;
x=p1*y+q1;
plot(x,y,'k-','linewidth',2);

%flap chord at nof:
y=linspace(nof1/bc*((p*bc+q)-cc+cr)-cr,nof1/bc*((p*bc+q)-cc+cr)-cr+cf1,N);
p1=0; q1=nof1;
x=p1*y+q1;
plot(x,y,'k-','linewidth',2);
hold on;

%upper part of flap 1:
x=linspace(nif1,nof1,N);
y=(x-nif1)/(nof1-nif1)*((nof1/bc*((p*bc+q)-cc+cr)-cr)-(nif1/bc*((p*bc+q)-cc+cr)-
cr))+nif1/bc*((p*bc+q)-cc+cr)-cr+cf1;
plot(x,y,'k-','linewidth',2);
hold on;

%flap2:

%flap chord at nif:
y=linspace((nif2-bc)/(b/2-bc)*(((p*bc+q)+tan(-freccia2*pi/180)*(b/2-bc))-
((p*bc+q)+tan(-freccia2*pi/180)*(bc-bc))+cc-ct)+((p*bc+q)+tan(-
freccia2*pi/180)*(bc-bc))-cc,(nif2-bc)/(b/2-bc)*(((p*bc+q)+tan(-
freccia2*pi/180)*(b/2-bc))-((p*bc+q)+tan(-freccia2*pi/180)*(bc-bc))+cc-
ct)+((p*bc+q)+tan(-freccia2*pi/180)*(bc-bc))-cc+cf2,N);
p1=0; q1=nif2;
x=p1*y+q1;
plot(x,y,'k-','linewidth',2);
%flap chord at nof:
y=linspace((nof2-bc)/(b/2-bc)*(((p*bc+q)+tan(-freccia2*pi/180)*(b/2-bc))-
((p*bc+q)+tan(-freccia2*pi/180)*(bc-bc))+cc-ct)+((p*bc+q)+tan(-
freccia2*pi/180)*(bc-bc))-cc,(nof2-bc)/(b/2-bc)*(((p*bc+q)+tan(-
freccia2*pi/180)*(b/2-bc))-((p*bc+q)+tan(-freccia2*pi/180)*(bc-bc))+cc-
ct)+((p*bc+q)+tan(-freccia2*pi/180)*(bc-bc))-cc+cf2,N);
p1=0; q1=nof2;
x=p1*y+q1;
plot(x,y,'k-','linewidth',2);
hold on;

```

```

%upper part of flap 1:
x=linspace(nif2,nof2,N);
y=(x-nif2)/(nof2-nif2)*((nof2-bc)/(b/2-bc)*((p*bc+q)+tan(-
freccia2*pi/180)*(b/2-bc))-((p*bc+q)+tan(-freccia2*pi/180)*(bc-bc))+cc-
ct)+((p*bc+q)+tan(-freccia2*pi/180)*(bc-bc))-cc)-((nif2-bc)/(b/2-
bc)*((p*bc+q)+tan(-freccia2*pi/180)*(b/2-bc))-((p*bc+q)+tan(-
freccia2*pi/180)*(bc-bc))+cc-ct)+((p*bc+q)+tan(-freccia2*pi/180)*(bc-bc))-
cc)+(nif2-bc)/(b/2-bc)*((p*bc+q)+tan(-freccia2*pi/180)*(b/2-bc))-
((p*bc+q)+tan(-freccia2*pi/180)*(bc-bc))+cc-ct)+((p*bc+q)+tan(-
freccia2*pi/180)*(bc-bc))-cc+cf2;
plot(x,y,'k-','linewidth',2);
hold on;

%slat 1:
slat(p,nisl,nosl,cs1,bc,freccia2);
hold on;

%slat2:
slat(p,nis2,nos2,cs2,bc,freccia2);

%slat 3:
slat(p,nis3,nos3,cs3,bc,freccia2);
hold on;

%slat 4:
slat(p,nis4,nos4,cs4,bc,freccia2);
hold on;

axis([-2 b/2+2 (b/2-bc)/(b/2-bc)*((p*bc+q)+tan(-freccia2*pi/180)*(b/2-bc))-
((p*bc+q)+tan(-freccia2*pi/180)*(bc-bc))+cc-ct)+((p*bc+q)+tan(-
freccia2*pi/180)*(bc-bc))-cc-4 4]);
end

function slat=slat(p,nis,nos,cs,bc,freccia2)

N=50;
q=0;
x=linspace(0,bc,N);
y=(p*bc+q)+tan(-freccia2*pi/180)*(x-bc);
%slat chord at nis:
y=linspace((p*bc+q)+tan(-freccia2*pi/180)*(nis-bc),(p*bc+q)+tan(-
freccia2*pi/180)*(nis-bc)-cs,N);
p1=0; q1=nis;
x=p1*y+q1;
plot(x,y,'k-','linewidth',2);

%slat chord at nos:
y=linspace((p*bc+q)+tan(-freccia2*pi/180)*(nos-bc),(p*bc+q)+tan(-
freccia2*pi/180)*(nos-bc)-cs,N);
p1=0; q1=nos;
x=p1*y+q1;
plot(x,y,'k-','linewidth',2);

%lower part of the slat:
x=linspace(nis,nos,N);
y=(x-nis)/(nos-nis)*((p*bc+q)+tan(-freccia2*pi/180)*(nos-bc))-((p*bc+q)+tan(-
freccia2*pi/180)*(nis-bc))+((p*bc+q)+tan(-freccia2*pi/180)*(nis-bc)-cs);
plot(x,y,'k-','linewidth',2);

end

```

## References

1. P. M. Sforza, *Commercial Airplane Design Principles*, 2014
2. E. Torenbeek, *Synthesis of Subsonic Airplane Design*, 1976
3. P. K. C. Rudolph, *High-Lift Systems on Commercial Subsonic Airliners*, 1996
4. J. D. Anderson Jr, *Aircraft Performance and Design*, 1999
5. <http://adg.stanford.edu/aa241/AircraftDesign.html>
6. [www.b737.org.uk/flightcontrols.htm](http://www.b737.org.uk/flightcontrols.htm)
7. [http://wpage.unina.it/fabrnic/DIDATTICA/PGV/PPT\\_2011/8\\_Ala\\_3.pdf](http://wpage.unina.it/fabrnic/DIDATTICA/PGV/PPT_2011/8_Ala_3.pdf)
8. [wpage.unina.it/agodemar/DSV-DQV/DSV-DQV\\_Quaderno\\_4.pdf](http://wpage.unina.it/agodemar/DSV-DQV/DSV-DQV_Quaderno_4.pdf)
9. [wpage.unina.it/agodemar/DSV-DQV/DSV-DQV\\_Quaderno\\_5.pdf](http://wpage.unina.it/agodemar/DSV-DQV/DSV-DQV_Quaderno_5.pdf)
10. [wpage.unina.it/agodemar/DSV-DQV/DSV-DQV\\_Quaderno\\_9.pdf](http://wpage.unina.it/agodemar/DSV-DQV/DSV-DQV_Quaderno_9.pdf)

## **Ringraziamenti**

Desideriamo ricordare tutti coloro che ci sono stati d'ausilio nella stesura della tesi con suggerimenti, critiche ed osservazioni: a loro va la nostra gratitudine.

Ringraziamo anzitutto il professor Fabrizio Nicolosi, Relatore, ed il professor Agostino De Marco che hanno, con la loro guida sapiente, saputo ascoltare ed interpretare le nostre esigenze, facilitando le nostre ricerche.

Un ringraziamento particolare va agli amici che ci hanno incoraggiato.

Vorremmo infine ringraziare le nostre famiglie che ci hanno sostenuti e supportato durante tutto il nostro percorso.